CTRP3 alleviates neuropathic pain by improving mitochondrial biogenesis and mitochondrial unfolded protein response via spinal SIRT1 in rats

TIANZHU LIU, LONGQING ZHANG and WEI MEI

Department of Anesthesiology and Pain Medicine, Hubei Key Laboratory of Geriatric Anesthesia and Perioperative Brain Health, and Wuhan Clinical Research Center for Geriatric Anesthesia, Tongji Hospital, Tongji Medical College, Huazhong University of Science and Technology, Wuhan, Hubei 430030, P.R. China

Received January 12, 2026; Accepted May 7, 2026

DOI: 10.3892/ijmm.2026.5868

Abstract. Neuropathic pain arises from an intricate network of interconnected pathophysiological mechanisms, yet the arsenal of effective therapeutic strategies remains frustratingly limited. Accumulating evidence has linked mitochondrial dysfunction to the progression of neuropathic pain. C1q-tumor necrosis factor-related protein-3 (CTRP3), a newly identified adipokine with diverse cytoprotective capacities, has not been previously explored for its role in nociceptive processing. To explore the role of CTRP3 in pain hypersensitivity, pain-related behavioral assessments were conducted using von Frey filaments and acetone drop method in male rats subjected to spared nerve injury (SNI). To unravel the underlying mechanisms, spinal cord tissues were subjected to western blotting, reverse transcription-quantitative PCR, immunofluorescence staining, dihydroethidium staining, small interfering RNA (siRNA) technologies and biochemical assays for quantifying oxidative markers. The findings showed that SNI markedly reduced endogenous CTRP3 expression in spinal neurons. Intrathecal administration of recombinant CTRP3 (rCTRP3) alleviated mechanical allodynia and cold hyperalgesia in SNI-induced rats. Additionally, rCTRP3 treatment enhanced PGC-1α-mediated mitochondrial biogenesis, ATF5-triggered mitochondrial unfolded protein response (UPR^{mt}), and mitigated spinal oxidative stress. Mechanistically, pharmacological inhibition of SIRT1 with EX-527, or siRNA-mediated silencing of PGC-1α or ATF5, reversed the effects of CTRP3 on pain hypersensitivity, mitochondrial biogenesis, UPR^{mt} and oxidative stress. The present study demonstrates that CTRP3 mitigates mechanical allodynia and cold hyperalgesia in male SNI rats by activating spinal SIRT1, thereby enhancing PGC-1α-mediated mitochondrial biogenesis and ATF5-induced UPR^{mt}. CTRP3 may therefore represent a novel therapeutic target for the management of neuropathic pain.

Introduction

Neuropathic pain, a debilitating chronic pain condition triggered by damage or dysfunction of the somatosensory nervous system, affects millions of individuals worldwide (1,2). Characterized by spontaneous pain, hyperalgesia and allodynia, this disorder often resists conventional analgesics, with current therapeutic options offering limited efficacy and frequent adverse effects (3-5). As such, unraveling the intricate pathophysiological mechanisms underlying neuropathic pain is critical for identifying novel therapeutic targets.

Mitochondrial biogenesis is pivotal for regulating mitochondrial DNA (mtDNA) replication, oxidative phosphorylation and ATP production, processes essential to sustaining mitochondrial function and homeostasis (6,7). It is orchestrated by nuclear and mitochondrial genes, with peroxisome proliferative activated receptor γ coactivator 1α (PGC-1α) serving as the master transcriptional co-activator (8). PGC-1α upregulates nuclear respiratory factor 1 (NRF1) and mitochondrial transcription factor A (TFAM), thereby driving expression of mtDNA and assembly of respiratory-chain complexes (9). Impaired mitochondrial biogenesis contributes to diverse diseases, including obesity (10), doxorubicin-induced cardiotoxicity (11), cerebral ischemia-reperfusion injury (12) and neurodegenerative disorders (13,14). The authors' previous studies also indicated that peripheral nerve injury-induced neuropathic pain suppresses mitochondrial biogenesis, while enhancing this process alleviates pain hypersensitivity (15,16). However, the specific mechanisms linking mitochondrial biogenesis to neuropathic pain remain incompletely understood.

Correspondence to: Professor Wei Mei or Dr Longqing Zhang, Department of Anesthesiology and Pain Medicine, Hubei Key Laboratory of Geriatric Anesthesia and Perioperative Brain Health, and Wuhan Clinical Research Center for Geriatric Anesthesia, Tongji Hospital, Tongji Medical College, Huazhong University of Science and Technology, 1095 Jiefang Avenue, Wuhan, Hubei 430030, P.R. China
E-mail: wmei@hust.edu.cn
E-mail: zlq@tjh.tjmu.edu.cn

Key words: C1q-tumor necrosis factor-related protein-3, neuropathic pain, mitochondrial biogenesis, mitochondrial unfolded protein response

The mitochondrial unfolded protein response (UPR^{mt}) represents a mitochondria-to-nucleus signaling pathway and acts as a cellular survival mechanism that gets triggered when the balance of mitochondrial protein homeostasis is perturbed (17-19). Its core function lies in preserving mitochondrial functionality by upregulating the transcription of chaperone proteins and proteases, which collectively regulate processes including protein folding, complex assembly and targeted degradation (18). Key molecular players involved in this regulatory network include the 10 kDa heat shock protein (Hsp10), 60 kDa heat shock protein (Hsp60), the proteolytic subunit of the ATP-dependent Clp protease (ClpP) and the mitochondrial Lon protease homolog (LonP1) (17). It can be activated by diverse factors through multiple regulatory pathways, such as activating transcription factor 5 (ATF5), a homolog of nematode ATFS-1 (18). Impaired UPR^{mt} elevates reactive oxygen species (ROS) levels, triggering oxidative stress and contributing to diseases such as osteoarthritis (OA) (20), Alzheimer's disease (21), cerebral ischemia (22) and traumatic brain injury (23). A recent study showed that enhancing UPR^{mt} with nicotinamide riboside (NR) improves mitochondrial function, reduces chondrocyte death, and alleviates OA pain; these effects notably were diminished in chondrocyte-specific ATF5-knockout mice (24). Additionally, it was found that the ATF5-mediated UPR^{mt} alleviated intervertebral disc degeneration via promoting mitophagy (25). However, the mechanisms linking UPR^{mt} to neuropathic pain remain poorly understood.

C1q-tumor necrosis factor-related protein-3 (CTRP3), a member of the adipokine CTRP family, has drawn attention for its pleiotropic cytoprotective effects (26,27). Beyond metabolic regulation, it exerts anti-inflammatory, antioxidant and tissue-protective properties in diverse pathological contexts, including cardiovascular disease (28), metabolic disorders (29) and intestinal inflammation disease (30). Recent research shows CTRP3 mitigates mitochondrial dysfunction and oxidative stress in pathological cardiac hypertrophy by activating the UPR^{mt} (31). Another study indicated that CTRP3 alleviates neurological deficits in cerebral ischemic stroke by promoting mitochondrial biogenesis (32). However, its specific role in pain hypersensitivity during neuropathic pain remains largely uninvestigated.

SIRT1, a NAD^+-dependent deacetylase belonging to the sirtuin family, regulates mitochondrial homeostasis by interacting with key transcriptional regulators (15,33). Recent studies show that aberrant SIRT1 expression reduces PGC-1α levels and impairs mitochondrial biogenesis (15,34). It may also activate the ATF5-mediated UPR^{mt}, protecting mitochondria from proteotoxic damage and mitigating oxidative stress (31,35). However, whether SIRT1 mediates CTRP3's regulatory effects on pain hypersensitivity, mitochondrial biogenesis, and UPR^{mt} in neuropathic pain remains unclear.

Against this backdrop, the present study sought to investigate the role of CTRP3 in neuropathic pain and explore its potential mechanisms of action. Using a rat model of spared nerve injury (SNI), it was examined whether CTRP3 regulates pain hypersensitivity by modulating mitochondrial function, and whether this effect is mediated through the SIRT1-PGC-1α/ATF5 signaling axis. By clarifying these relationships, it was aimed to shed light on novel therapeutic strategies for neuropathic pain targeting CTRP3 and its downstream pathways.

Materials and methods

Animals. Male Sprague-Dawley (SD) rats aged 6-7 weeks (weighing 250-280 g; total number: n=315 rats) were purchased from the experimental animal center of Tongji Hospital, Tongji Medical College, Huazhong University of Science and Technology. All rats were housed in the specific pathogen-free animal facility, under controlled environmental conditions: Temperature maintained at 23±1˚C, relative humidity at 50±10%, and a 12/12-h light/dark cycle. Rats were group-housed (2 per cage) in polypropylene cages with autoclaved wood chip bedding and provided with standard rodent chow and sterile water *ad libitum*. All experimental procedures were approved by the Experimental Animal Care and Use Committee of Tongji Hospital, Tongji Medical College, Huazhong University of Science and Technology (approval no. TJH-202106615; Wuhan, China). The study was conducted in accordance with the ARRIVE guidelines to ensure transparency and reproducibility. All experiments were carried out under blinded conditions. Rats were randomly assigned to distinct groups, with syringes holding different drugs randomly coded by an independent researcher; injections were then administered strictly according to these codes. Behavioral assessments were conducted without the assessors knowing which treatment each group received.

Neuropathic pain model. Neuropathic pain was induced in rats using the SNI model, as previously described (15). Rats were anesthetized with isoflurane (induction, 5%; maintenance, 2-3%; cat. no. R510-22-10, RWD) and placed on a 37˚C heating pad. The left hindlimb was shaved and disinfected, followed by a 1.5-2-cm incision along the thigh to expose the sciatic nerve and its three branches (common peroneal, tibial and sural). The common peroneal and tibial nerves were ligated with 6-0 silk sutures (5 mm apart), transected, and 2 mm of distal stumps were removed; the sural nerve was spared. Muscles and skin were sutured with 4-0 absorbable and 5-0 nylon sutures, respectively. After surgery, rats were allowed to recover in individual cages with free access to food and water. Sham-operated rats underwent the same exposure but without nerve ligation/transections.

Pain behavioral testing. Mechanical pain sensitivity was evaluated using the von Frey test (36). All tests were performed by a blinded experimenter in a quiet room. Rats were acclimatized to Plexiglas chambers on a wire mesh floor for 30 min before testing. Von Frey filaments (1.0-15.0 g) were applied vertically to the ipsilateral hindpaw plantar surface for 5 sec. A positive response (paw withdrawal, flinching, or licking) prompted using a weaker filament; no response prompted a stronger one. Using the up-down method, paw withdrawal threshold (PWT, 50% withdrawal threshold) was calculated after 6 measurements. Each paw was tested 3 times (5-min intervals), and the mean was recorded. Cold hyperalgesia was assessed using the acetone drop method, as previously described (37). Prior to testing, rats were individually housed in transparent plastic observation chambers with a wire-mesh floor and allowed a

30-min habituation period to minimize environmental stress. Following acclimatization, a 0.1-ml syringe was used to form an acetone bubble, which was gently applied to the plantar surface of the left hind paw. This procedure was repeated three times per paw, with a 5-min interval between consecutive applications to avoid sensory adaptation. During each trial, the cumulative duration of paw-related nocifensive behaviors, including licking, biting, and lifting the paw off the mesh floor, was recorded. The paw withdrawal cold duration (PWCD) for each rat was determined as the mean value derived from six independent trials.

Intrathecal catheterization. Intrathecal catheterization was performed as previously described (38). Rats were anesthetized with isoflurane (induction, 5%; maintenance, 2-3%) and placed in a stereotaxic frame in a prone position. The atlanto-occipital membrane was exposed via a midline incision at the base of the skull. A PE-10 polyethylene catheter filled with sterile saline was inserted through the membrane into the subarachnoid space at the lumbar enlargement (L5-L6 level). The catheter was secured to the surrounding tissues with 4-0 silk sutures, and the free end was exteriorized at the back of the neck, sealed with a stainless-steel obturator, and protected by a plastic cap. Successful catheter placement was verified by injecting 10 μl of sterile saline containing 2% lidocaine. A transient (30-60 sec) bilateral hindlimb paralysis indicated correct positioning. Rats were allowed a 7-day recovery period before experimental use.

Drug administration. Recombinant CTRP3 (rCTRP3; cat. no. 9398-TN; Novus Biologicals, LLC) and EX-527 (a selective SIRT1 inhibitor; cat. no. HY-15452; MedChemExpress) were administered via intrathecal injection. rCTRP3 was dissolved in sterile physiological saline to prepare working solutions at concentrations corresponding to three doses: 10 μg/rat, 30 μg/rat and 90 μg/rat. Intrathecal injections were performed daily for 7 consecutive days starting from 7 day after SNI surgery. The injection volume was adjusted to 5 μl per rat, followed by 5 μl PBS to ensure complete delivery. To investigate the role of SIRT1 in CTRP3-mediated effects, the selective SIRT1 inhibitor EX-527 was used. EX-527 was dissolved in 10% dimethyl sulfoxide and administered at a fixed dose of 1.5 μg per rat. The dose of EX-527 was chosen according to a previous study (15). Intrathecal injection of EX-527 was performed 30 min prior to rCTRP3 administration in the respective experimental groups. At the end point of experiment, rats were euthanized by intraperitoneal injection of an overdose of pentobarbital sodium at a dose of 150 mg/kg body weight (39). Death was confirmed by respiratory/cardiac arrest, dilated pupils, and absent corneal reflex.

Intrathecal injection of small interfering RNA (siRNA). siRNAs targeting PGC-1α (PGC-1α siRNA) and ATF5 (ATF5 siRNA), along with non-targeting scrambled siRNA (negative control), were used to silence the expression of these genes in the spinal cord. All siRNAs were purchased from TsingKe Biological Technology. The sequences of siRNAs are listed in Table SI. To verify the knockdown efficiency and specificity of PGC-1α siRNA and ATF5 siRNA, independent *in vitro* validation was performed in PC12 cells. Cells were transfected with PGC-1α siRNA or ATF5 siRNA using Lipofectamine 3000 transfection reagent (cat. no. L3000008; Invitrogen; Thermo Fisher Scientific, Inc.), as previously described (40). The knockdown efficiency was verified by reverse transcription-quantitative PCR (RT-qPCR). For *in vivo*, the siRNA was dissolved in RNase-free water at 2.5 μg/μl and mixed with the transfection reagent branched polyethyleneimine (PEI; cat. no. 408727; MilliporeSigma). Intrathecal injection of siRNA in a total volume of 5 μl was initiated 5-11 days post SNI, and the knockdown efficiency of PGC-1α and ATF5 was verified by RT-qPCR (38).

RT-qPCR. Total RNA was extracted from the L4-L6 segments of the spinal cord using RNA Extraction kit (cat. no. R701-01; Vazyme Biotech Co., Ltd.) following the manufacturer's protocol (41). The complementary DNA (cDNA) was synthesized using a reverse transcription reagent kit (cat. no. R212-01; Vazyme Biotech Co., Ltd.), following the manufacturer's protocols. Amplifications were run on a Real-Time PCR System (Applied Biosystems QuantStudio 6; Thermo Fisher Scientific, Inc.). The reaction mixture (20 μl total volume) contained 10 μl of SYBR Green Supermix (cat. no. 172515; Bio-Rad Laboratories, Inc.), 0.4 μl of forward primer, 0.4 μl of reverse primer, 2 μl of cDNA template, and 7.2 μl of nuclease-free water. The thermal cycling conditions were as follows: Initial denaturation at 95˚C for 30 sec, followed by 40 cycles of denaturation at 95˚C for 5 sec and annealing/extension at 60˚C for 30 sec. Primers for target genes and the reference gene (β-actin) were synthesized by TsingKe Biological Technology. The primer sequences are listed in Table SII. Relative mRNA expression levels were calculated using the $2^{-\Delta\Delta Cq}$ method, with β-actin serving as the internal reference to normalize target gene expression (42).

Immunofluorescence (IF) staining. IF staining was conducted according to a previous study (43). Spinal cord segments (L4-L6) were harvested and immediately fixed in 4% paraformaldehyde (PFA) in 0.01 M phosphate-buffered saline (PBS) at 4˚C for 24 h. After fixation, tissues were transferred to 30% sucrose solution (in 0.01 M PBS) for cryoprotection at 4˚C, with solution changes every 24 h until tissues fully sank. Transverse frozen sections (20-μm thickness) were cut using a cryostat microtome (Leica Microsystems GmbH). To permeabilize cell membranes and block non-specific binding, sections were incubated in blocking buffer (5% bovine serum albumin (Wuhan Boster Biological Technology, Ltd.) + 0.3% Triton X-100 in 0.01 M PBS) at 25˚C for 1 h. Primary antibodies were diluted in blocking buffer and applied to sections, which were then incubated overnight at 4˚C in a humidified chamber. The following day, sections were washed with 0.01 M PBS and incubated with a mixture of second antibodies at 25˚C for 1 h in the dark. The antibodies used in IF staining are listed in Table SIII. Images were acquired using a fluorescence microscope (Olympus Corporation). The results were expressed as the number of double-positive cells per square millimeter and quantified using ImageJ 1.8 software (National Institutes of Health), as previously described (38).

Western blotting (WB). WB analysis was performed as previously described (15). Spinal cord tissues (L4-L6 segments) were homogenized in RIPA (Wuhan Boster Biological Technology,

Ltd.; main components: 1% TritonX-100, 1% Sodium deoxycholate, 0.1% SDS) lysis buffer (containing 1% protease and phosphatase inhibitor cocktail) on ice, at a ratio of 1 g tissue to 10 ml buffer. After centrifugation at 12,000 x g for 15 min at 4˚C, the supernatant was collected, and protein concentration was determined using a BCA protein assay kit (Thermo Fisher Scientific, Inc.). Equal amounts of protein (50 μg per sample) were separated by 10% SDS-PAGE and transferred to polyvinylidene difluoride membranes. Membranes were blocked with 5% non-fat milk in Tris-buffered saline with 0.1% Tween-20 (TBST) for 1 h at 25˚C, then incubated overnight at 4˚C with primary antibodies. After washing with 10% TBST, the membranes were incubated with second antibodies for 1 h at 25˚C. The antibodies used in WB are listed in Table SIV. Protein bands were visualized using an enhanced chemiluminescence (ECL) detection kit (Millipore) and imaged with a ChemiDoc XRS+ system (Bio-Rad Laboratories, Inc.). Band intensities were quantified using ImageLab software 5.2 (Bio-Rad Laboratories, Inc.), with target protein expression normalized to β-actin.

mtDNA copy number quantification. The mtDNA copy number quantification was performed as previously described (15). Total DNA was extracted from L4-L6 spinal cord segments using a Tissue Genomic DNA Extraction Kit [Elk (Wuhan) Biotechnology Co., Ltd.] following the manufacturer's protocol, and mtDNA copy number was determined by RT-qPCR using primers specific for mitochondrial genes and a nuclear reference gene. Relative mtDNA copy number was assessed by the mitochondrial encoded NADH dehydrogenase 1 (ND1) and was normalized to nuclear-encoded β-actin. The primer sequences are listed in Table SII.

Dihydroethidium (DHE) staining. Superoxide anions were detected using DHE staining, following the previously described method (36,44). Frozen sections (20-μm thickness) of the L4-L6 spinal cord segments were prepared. These sections were incubated with 1.5 μmol/ml DHE (cat. no. HY-D0079; MedChemExpress) at 25˚C for 50 min in a dark environment. Subsequently, the sections were stained with 4',6-diamidino-2-phenylindole (DAPI) at a concentration of 0.001 mg/ml at 25˚C for 10 min in the dark. Images were acquired using a fluorescence microscope (Olympus Corporation). For DHE staining analysis, the number of DHE-positive cells per square millimeter was counted, and the data were processed using ImageJ 1.8 software (National Institutes of Health).

Biochemical assays for oxidative stress and antioxidant markers. Oxidative stress parameters and antioxidant indices were measured using commercial kits, following procedures similar to those previously described (36). Tissue samples were homogenized and centrifuged at 16,000 x g for 30 min at 4˚C, with the supernatants collected for subsequent biochemical assays. The resulting supernatant was collected for subsequent analyses, with protein concentrations determined via BCA assay to normalize the results. Levels of oxidative damage markers, including malondialdehyde (MDA) and protein carbonyl (PCO), were quantified using the corresponding assay kits respectively, in strict accordance with the manufacturers' protocols. For antioxidant indices, glutathione (GSH) levels, superoxide dismutase (SOD) activity and glutathione peroxidase (GSH-PX) activity were assessed using the corresponding assay kits respectively, following the manufacturer's instructions. The commercial assay kits used in biochemical assays are listed in Table SV.

Mitochondrial membrane potential (MMP) measurement. Mitochondria were isolated from rat spinal cord tissues using a mitochondrial isolation kit (cat. no. ab110168; Abcam) according to the manufacturer's instructions. Briefly, tissue samples were homogenized in ice-cold isolation buffer, and the homogenate was centrifuged at low speed to remove debris. The supernatant was then centrifuged at high speed to obtain the mitochondrial pellet, which was washed and resuspended in assay buffer. For MMP detection, the isolated mitochondria were incubated with 5 μM JC-1 dye (cat. no. C2003S; Beyotime Institute of Biotechnology) at 37˚C for 30 min in the dark. Fluorescence intensities were measured by flow cytometry (BD FACSCanto II; BD Biosciences), and MMP was calculated as the ratio of red fluorescence (aggregated JC-1) to green fluorescence (monomeric JC-1) using FlowJo software (version 10.8.1; Tree Star, Inc.).

Measurement of ATP levels. ATP levels were measured using an ATP Assay Kit (cat. no. S0026; Beyotime Institute of Biotechnology), as previously described (45). Briefly, spinal cord tissues were homogenized in lysis buffer, and the homogenate was centrifuged at 12,000 x g for 5 min at 4˚C. The supernatant was collected and mixed with ATP detection working solution, and the luminescence intensity was determined using a microplate reader. The ATP concentration was calculated according to a standard curve. Protein concentration was measured using a BCA Protein Assay Kit, and ATP levels were normalized to total protein content and expressed as nmol/mg protein.

Statistical analysis. All data are presented as the mean ± standard error of the mean (SEM). Statistical analyses were performed using GraphPad Prism 9.0 software (Dotmatics). Normality distribution was evaluated using the Shapiro-Wilk test. For comparisons between two groups, unpaired Student's t-test was used. For multiple group comparisons, one-way analysis of variance (ANOVA) was applied, followed by Bonferroni's post hoc test for multiple comparison correction. Behavioral data were analyzed using two-way repeated-measures ANOVA, with group (row factor) and time (column factor) as the main factors, and interaction between group and time was also tested. $P<0.05$ was considered to indicate a statistically significant difference. Effect sizes were reported as eta squared (η^2, representing partial eta squared) for all main effects, interactions, and two-sample t-tests. Relevant statistical results have been incorporated into the following section.

Results

Expression of CTRP3 in the spinal cord following SNI. A neuropathic pain model was established using the SNI procedure. As depicted in Fig. 1A [Interaction:

F (3, 72)=17.45, P<0.0001, η^2=0.4211; Time factor: F (3, 72)=20.39, P<0.0001, η^2=0.4593; Group factor: F (1, 72)=207.9, P<0.0001, η^2=0.7428] and Fig. 1B [Interaction: F (3, 72)=24.09, P<0.0001, η^2=0.5010; Time factor: F (3, 72)=25.93, P<0.0001, η^2=0.5193; Group factor: F (1, 72)=194.6, P<0.0001, η^2=0.7299], behavioral pain testing results indicated that, relative to sham-operated controls, rats receiving SNI displayed a statistically significant decrease in PWT and a concurrent increase in PWCD over the time window of post-operative day 3 to day 14, confirming the successful induction of neuropathic pain hypersensitivity. To assess changes in CTRP3 expression, RT-qPCR and WB analyses were performed on spinal cord tissues. The results revealed that SNI led to a downregulation of both CTRP3 mRNA [Fig. 1C: F (3, 16)=47.17, P<0.0001, η^2=0.8984] and protein [Fig. 1D: F (3, 16)=51.68, P<0.0001, η^2=0.9065] levels in the spinal cord compared with the sham-operated group. Furthermore, IF staining was employed to determine the cellular localization of CTRP3 in the spinal dorsal horn. As shown in Fig. 1E-I [Fig. 1G: t (8)=14.17, P<0.0001, η^2=0.9617; Fig. 1H: t (8)=2.194, P=0.0595, η^2=0.3757; Fig. 1I: t (8)=1.965, P=0.0850, η^2=0.3255], CTRP3 was predominantly localized in neurons (identified by NeuN) within the spinal dorsal horn. Notably, the number of CTRP3-positive neurons was significantly reduced post-SNI relative to the sham group. These findings suggest that neuronal CTRP3 in the spinal cord may play a critical role in the development of SNI-induced neuropathic pain in male rats.

Treatment with rCTRP3 alleviates pain hypersensitivity in SNI rats mediated by SIRT1. To further investigate the role of CTRP3 in neuropathic pain, intrathecal injections of rCTRP3 at doses of 10, 30, or 90 μg were administered from day 7 to day 11 post-nerve injury. As shown in Fig. 2A [Interaction: F (20, 270)=3.781, P<0.0001, η^2=0.2187; Time factor: F (5, 270)=45.32, P<0.0001, η^2=0.4562; Group factor: F (4, 270)=115.9, P<0.0001, η^2=0.6319] and Fig. 2B [Interaction: F (20, 270)=4.618, P<0.0001, η^2=0.2548; Time factor: F (5, 270)=41.57, P<0.0001; η^2=0.4350; Group factor: F (4, 270)=124.8, P<0.0001, η^2=0.6489], repeated intrathecal administration of rCTRP3 at 30 and 90 μg significantly restored the reduced PWT and abrogated the elevated PWCD relative to the SNI + vehicle group. These results demonstrated that repeated rCTRP3 administration could mitigate established mechanical allodynia and cold hyperalgesia in SNI rats. Additionally, IF staining and WB analyses were used to assess spinal SIRT1 expression. IF staining results revealed that the number of SIRT1-positive neurons was decreased after SNI compared with the sham group, while treatment with rCTRP3 (30 and 90 μg) reversed this reduction in SIRT1 expression in spinal dorsal horn neurons of SNI rats [Fig. 2C and D: F (4, 20)=13.83, P<0.0001, η^2=0.7344]. Consistently, WB results showed that rCTRP3 administration (30 and 90 μg) blocked the nerve injury-induced downregulation of SIRT1 in the spinal cord, relative to the SNI + vehicle group [Fig. 2E: F (4, 20)=10.86, P<0.0001, η^2=0.6847]. These findings confirm that CTRP3 alleviates SNI-induced mechanical allodynia and cold hyperalgesia and suggest that neuronal SIRT1 in the spinal cord may mediate this analgesic effect in SNI rats.

Intrathecal injection with rCTRP3 promotes mitochondrial biogenesis in SNI rats. Mitochondrial biogenesis is a key process for sustaining mitochondrial homeostasis. It was hypothesized that the analgesic effect of rCTRP3 may involve the regulation of mitochondrial biogenesis. To test this, targets associated with mitochondrial biogenesis were examined, including PGC-1α (a critical inducer of mitochondrial biogenesis), NRF1, TFAM and mtDNA copy number. As demonstrated in Fig. 3A and B [F (4, 20)=12.33, P<0.0001, η^2=0.7115], IF staining revealed that the number of PGC-1α-positive neurons in the spinal dorsal horn was reduced after SNI compared with the sham group, whereas treatment with rCTRP3 (30 and 90 μg) reversed this decrease in PGC-1α expression in SNI rats. Consistently, WB analysis demonstrated that rCTRP3 administration (30 and 90 μg) blocked the nerve injury-induced downregulation of PGC-1α [Fig. 3C: F (4, 20)=16.94, P<0.0001, η^2=0.7721], NRF1 [Fig. 3D: F (4, 20)=14.79, P<0.0001, η^2=0.7473] and TFAM [Fig. 3E: F (4, 20)=12.68, P<0.0001, η^2=0.7172] in the spinal cord, relative to the SNI + vehicle group. Additionally, mtDNA copy number was measured to assess mitochondrial biogenesis activity. As revealed in Fig. 3F [F (4, 20)=18.68, P<0.0001, η^2=0.7888], rCTRP3 treatment (30 and 90 μg) reversed the reduction in spinal mtDNA copy number observed in SNI rats. These findings confirm that CTRP3 enhances PGC-1α-dependent mitochondrial biogenesis in the spinal cord of SNI-induced rats.

Intrathecal delivery of rCTRP3 facilitates UPR^{mt} in SNI rats. The UPR^{mt} is a vital mechanism for maintaining mitochondrial protein homeostasis and redox balance. It was hypothesized that CTRP3 may exert its analgesic effects partly through the regulation of UPR^{mt}. To explore this, UPR^{mt}-related targets were analyzed, including ATF5 (a key inducer of UPR^{mt}), chaperone proteins (Hsp60) and proteases (ClpP, LonP1). As shown in Fig. 4A and B [F (4, 20)=10.88, P<0.0001, η^2=0.6851], IF staining indicated that the number of ATF5-positive neurons in the spinal dorsal horn was decreased after SNI compared with the sham group, while rCTRP3 treatment (30 and 90 μg) reversed this reduction in ATF5 expression in SNI rats. Consistently, RT-qPCR results demonstrated that rCTRP3 administration (30 and 90 μg) blocked the nerve injury-induced downregulation of ATF5 [Fig. 4C: F (4, 20)=19.39, P<0.0001, η^2=0.7950], ClpP [Fig. 4D: F (4, 20)=15.12, P<0.0001, η^2=0.7515], Hsp60 [Fig. 4E: F (4, 20)=13.06, P<0.0001, η^2=0.7231] and LonP1 [Fig. 4F: F (4, 20)=11.67, P<0.0001, η^2=0.7001] in the spinal cord, relative to the SNI + vehicle group. These results confirm that CTRP3 promotes ATF5-mediated UPR^{mt} in the spinal cord of SNI-induced rats.

Administration of rCTRP3 mitigates spinal mitochondrial dysfunction and oxidative stress in SNI rats. To further verify the protective effects of rCTRP3 on mitochondrial function, MMP and intracellular ATP production were directly measured. As illustrated in Fig. S1A-C, SNI induced a marked reduction in MMP [F (4, 20)=31.33, P<0.0001, η^2=0.8624] and ATP levels [F (4, 20)=14.26, P<0.0001, η^2=0.7404] in the spinal cord, both of which were significantly restored by intrathecal administration of rCTRP3 at 30 and 90 μg. These data provide

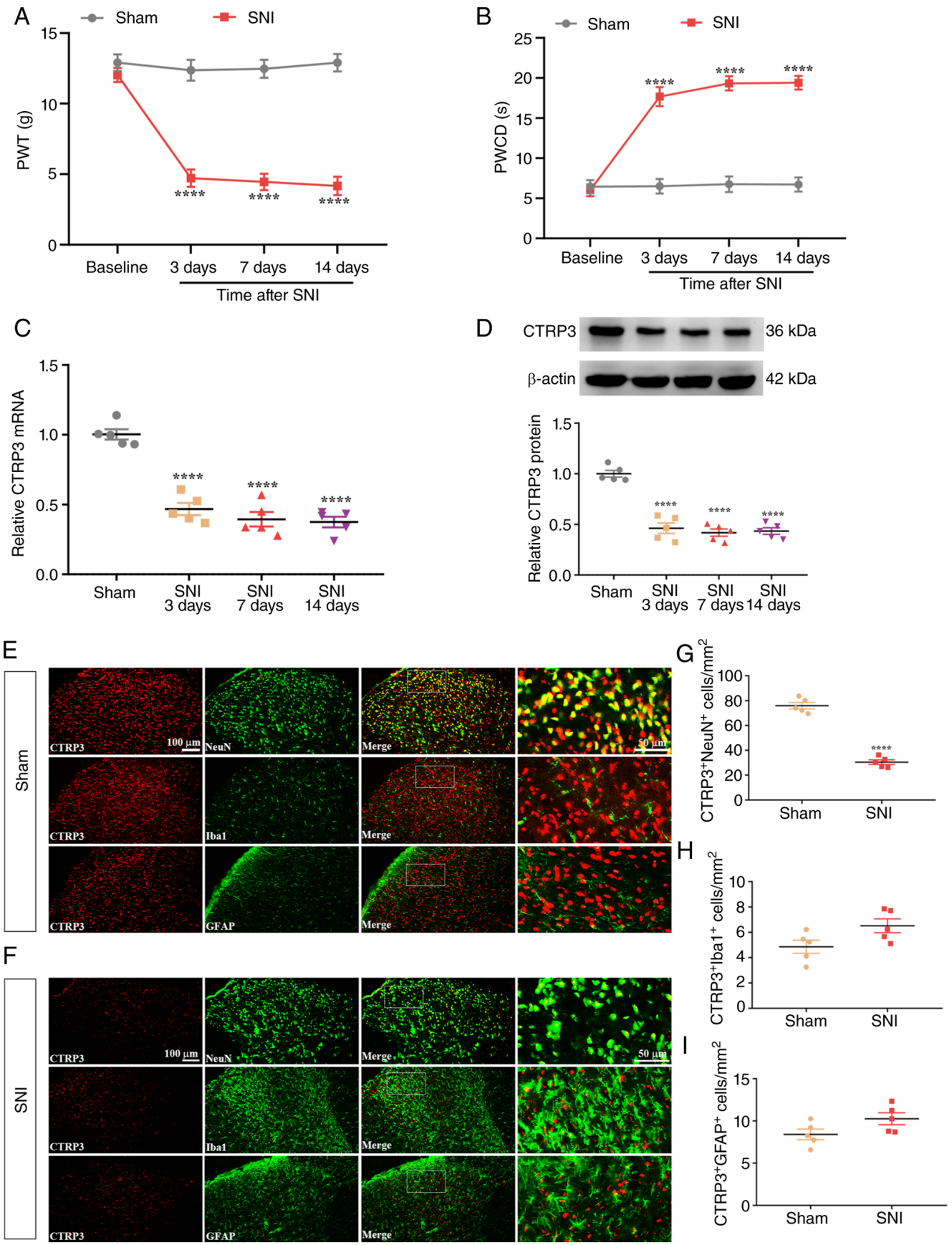

Figure 1. Spinal CTRP3 expression is downregulated following SNI. (A and B) Compared with sham-operated control rats, rats subjected to SNI exhibited a significant reduction in PWT and a prominent elevation in PWCD from post-SNI day 3 to day 14. ****P<0.0001 vs. sham group, n=10 rats/group. (C and D) RT-qPCR and WB analyses showed a marked decrease in CTRP3 mRNA and protein levels in the spinal cord of SNI rats relative to sham controls. (E-I) IF staining results demonstrated that SNI led to reduced CTRP3 expression in neurons within the spinal dorsal horn of rats. ****P<0.0001 vs. sham group, n=5 rats/group. SNI, spared nerve injury; PWT, paw withdrawal threshold; PWCD, paw withdrawal cold duration; RT-qPCR, reverse transcription-quantitative polymerase chain reaction; WB, western blotting; IF, immunofluorescence; CTRP3, C1q-tumor necrosis factor-related protein 3.

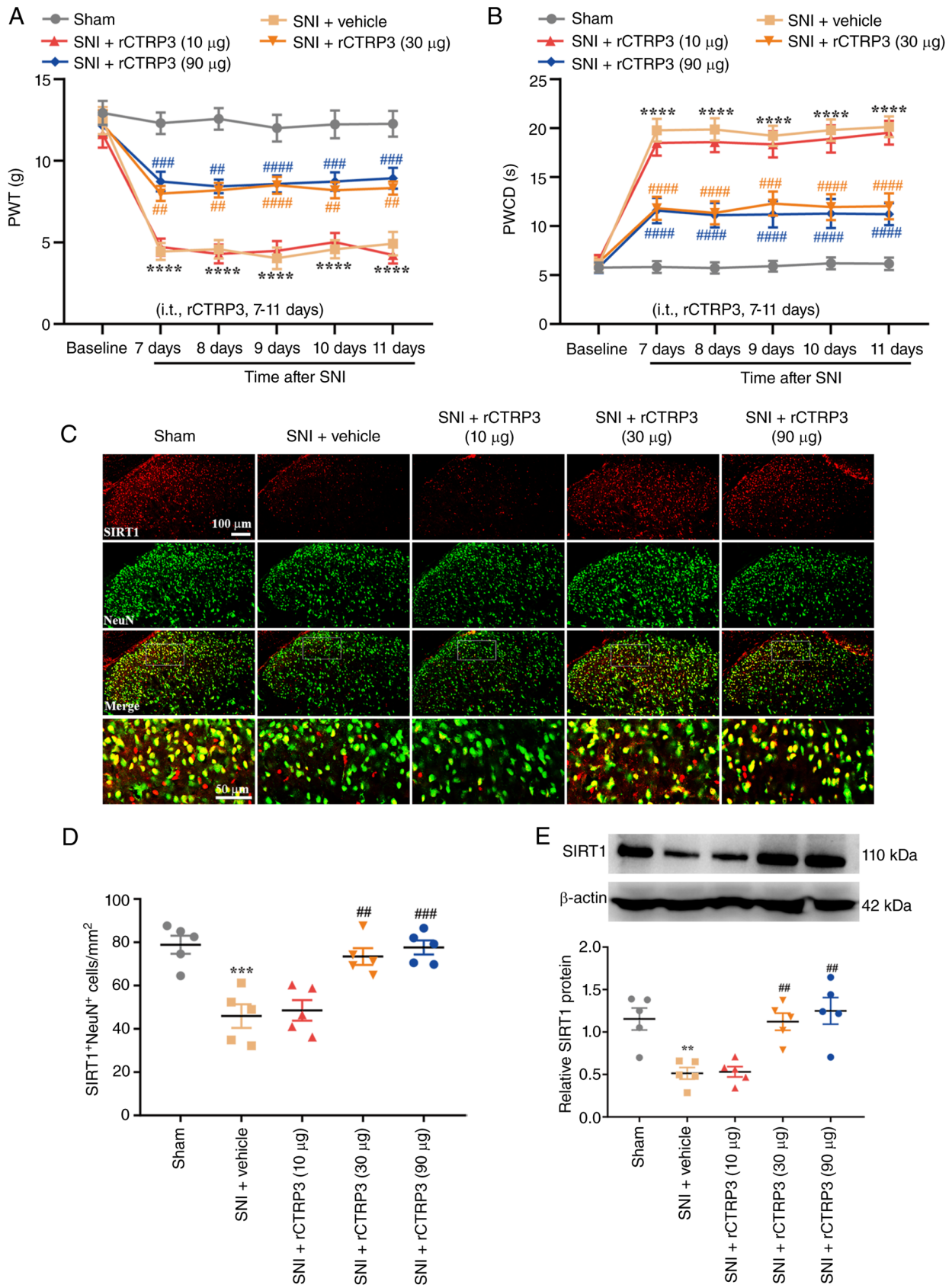

Figure 2. Intrathecal administration of rCTRP3 alleviates pain hypersensitivity and activates spinal SIRT1 in SNI rats. (A and B) Behavioral assessments showed that repeated intrathecal injection of rCTRP3 (30 or 90 μg) significantly reversed the SNI-induced reductions in PWT and increases in PWCD. ****P<0.0001 vs. sham group; $^{\#\#}$P<0.01, $^{\#\#\#}$P<0.001 and $^{\#\#\#\#}$P<0.0001 vs. SNI + vehicle group; n=10 rats/group. (C and D) IF staining results revealed that the number of SIRT1-positive neurons was lower in SNI rats than in the sham group, whereas treatment with rCTRP3 (30 and 90 μg) reversed this decrease in SIRT1 expression in spinal dorsal horn neurons of SNI rats. (E) WB analysis demonstrated that SIRT1 levels in the spinal cord were reduced in SNI rats, and this downregulation was markedly attenuated by rCTRP3 treatment at doses of 30 or 90 μg. **P<0.01 and ***P<0.001 vs. sham group; $^{\#\#}$P<0.01 and $^{\#\#\#}$P<0.001, vs. SNI + vehicle group; n=5 rats/group. rCTRP3, recombinant complement C1q tumor necrosis factor-related protein 3; SNI, spared nerve injury; PWT, paw withdrawal threshold; PWCD, paw withdrawal cold duration; IF, immunofluorescence; SIRT1, sirtuin 1; WB, western blotting.

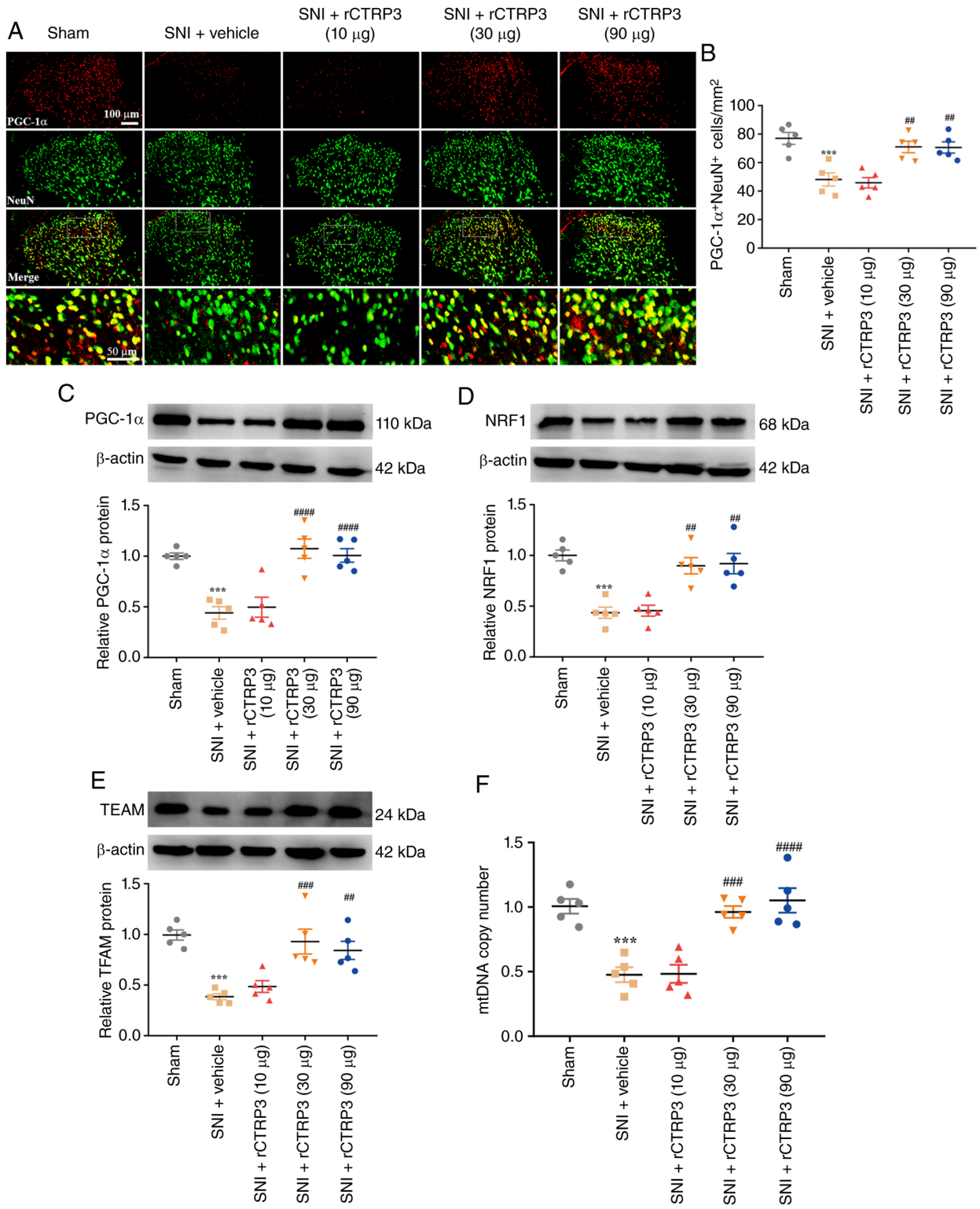

Figure 3. rCTRP3 promotes PGC-1α-mediated mitochondrial biogenesis in the spinal cord of SNI rats. (A and B) IF staining showed a significant decrease in neuronal PGC-1α levels in SNI rats; this reduction was notably reversed by intrathecal administration of rCTRP3 (30 and 90 μg). (C-E) WB analysis demonstrated that rCTRP3 treatment (30 and 90 μg) blocked the nerve injury-induced downregulation of PGC-1α, NRF1 and TFAM in the spinal cord, compared with the SNI + vehicle group. (F) rCTRP3 administration (30 and 90 μg) reversed the reduction in spinal mtDNA copy number observed in SNI rats. ***P<0.001 vs. sham group; $^{\#\#}$P<0.01, $^{\#\#\#}$P<0.001 and $^{\#\#\#\#}$P<0.0001 vs. SNI + vehicle group; n=5 rats/group. rCTRP3, recombinant complement C1q tumor necrosis factor-related protein 3; PGC-1α, peroxisome proliferator-activated receptor gamma coactivator 1-alpha; SNI, spared nerve injury; IF, immunofluorescence; WB, western blotting; NRF1, nuclear respiratory factor 1; TFAM, mitochondrial transcription factor A; mtDNA, mitochondrial DNA.

direct functional evidence that rCTRP3 preserves mitochondrial bioenergetic capacity in the setting of neuropathic pain. Redox balance in the spinal cord was evaluated using DHE staining and biochemical assays. As revealed in Fig. 5A and B [F (4, 20)=69.93, P<0.0001, η^2=0.9333], DHE staining results revealed that administration of rCTRP3 (30 and 90 μg) reduced

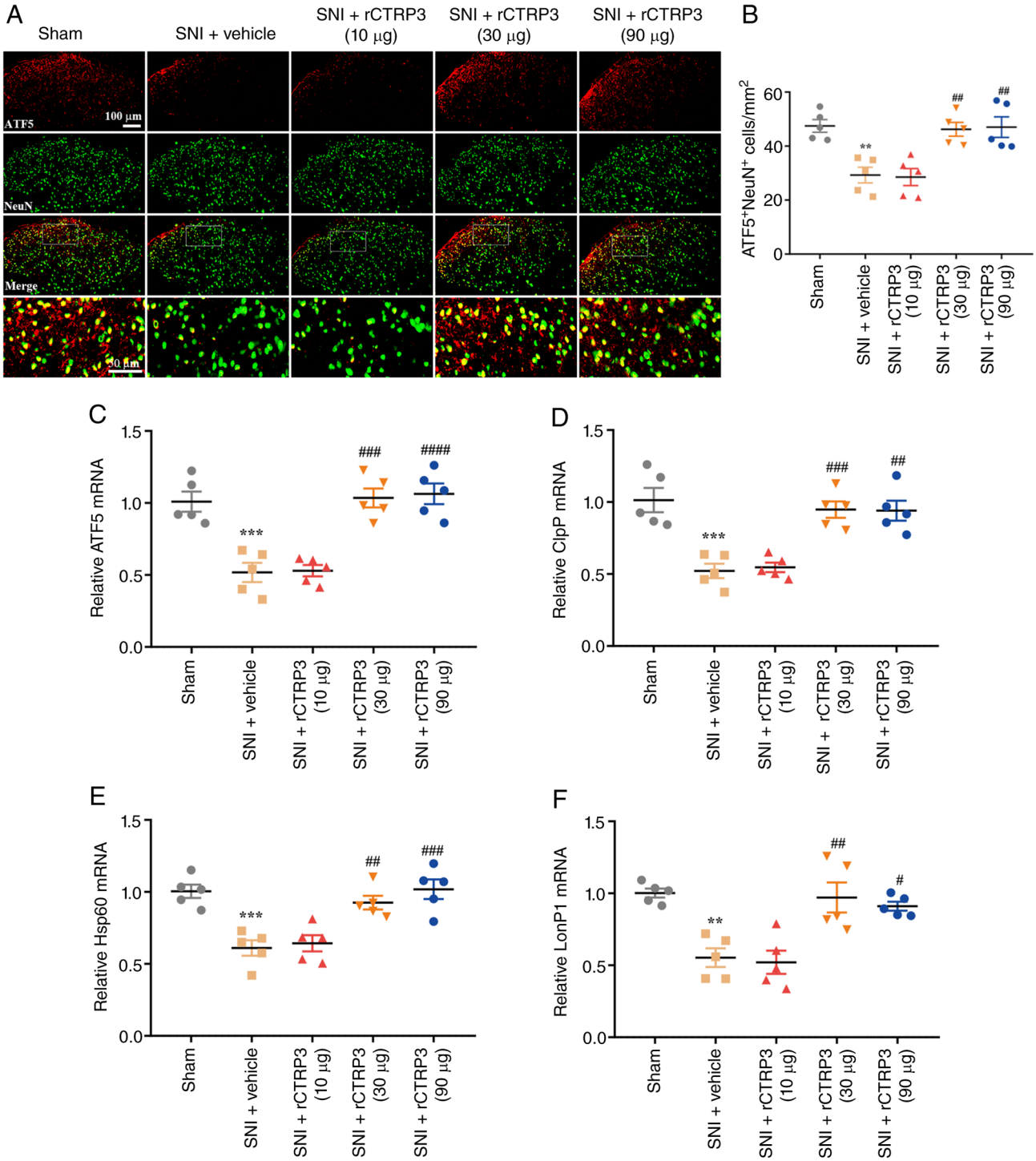

Figure 4. rCTRP3 promotes ATF5-induced UPR^{mt} in the spinal cord of SNI rats. (A and B) IF staining showed a notable decrease in spinal neuronal ATF5 levels in SNI rats; this reduction was significantly reversed by intrathecal administration of rCTRP3 (30 and 90 μg). (C-F) RT-qPCR analysis demonstrated that rCTRP3 treatment (30 and 90 μg) blocked the nerve injury-induced downregulation of ATF5, ClpP, Hsp60 and LonP1 in the spinal cord, compared with the SNI + vehicle group. **P<0.01 and ***P<0.001 vs. sham group; $^{\#}$P<0.05, $^{\#\#}$P<0.01, $^{\#\#\#}$P<0.001 and $^{\#\#\#\#}$P<0.0001 vs. SNI + vehicle group; n=5 rats/group. rCTRP3, recombinant complement C1q tumor necrosis factor-related protein 3; ATF5, activating transcription factor 5; UPR^{mt}, mitochondrial unfolded protein response; SNI, spared nerve injury; IF, immunofluorescence; RT-qPCR, reverse transcription-quantitative polymerase chain reaction; ClpP, caseinolytic mitochondrial matrix peptidase proteolytic subunit; Hsp60, heat shock protein 60; LonP1, Lon protease 1.

the number of DHE-positive cells in the spinal cord of SNI rats, which was elevated in the SNI + vehicle group. Consistent with this, biochemical assay data demonstrated that rCTRP3 treatment (30 and 90 μg) reversed the SNI-induced increases in oxidative damage markers, including MDA [Fig. 5C: F (4, 20)=16.82, P<0.0001, η^2=0.7709] and PCO [Fig. 5D: F (4, 20)=16.88, P<0.0001, η^2=0.7715] in the spinal cord. Additionally, rCTRP3 intervention (30 and 90 μg) significantly increased the level of reduced GSH [Fig. 5E: F (4, 20)=11.99, P<0.0001, η^2=0.7056] and enhanced the activity of antioxidant enzymes, including GSH-PX [Fig. 5F: F (4, 20)=13.09, P<0.0001, η^2=0.7236] and SOD [Fig. 5G: F (4, 20)=10.52, P<0.0001, η^2=0.6779] in the

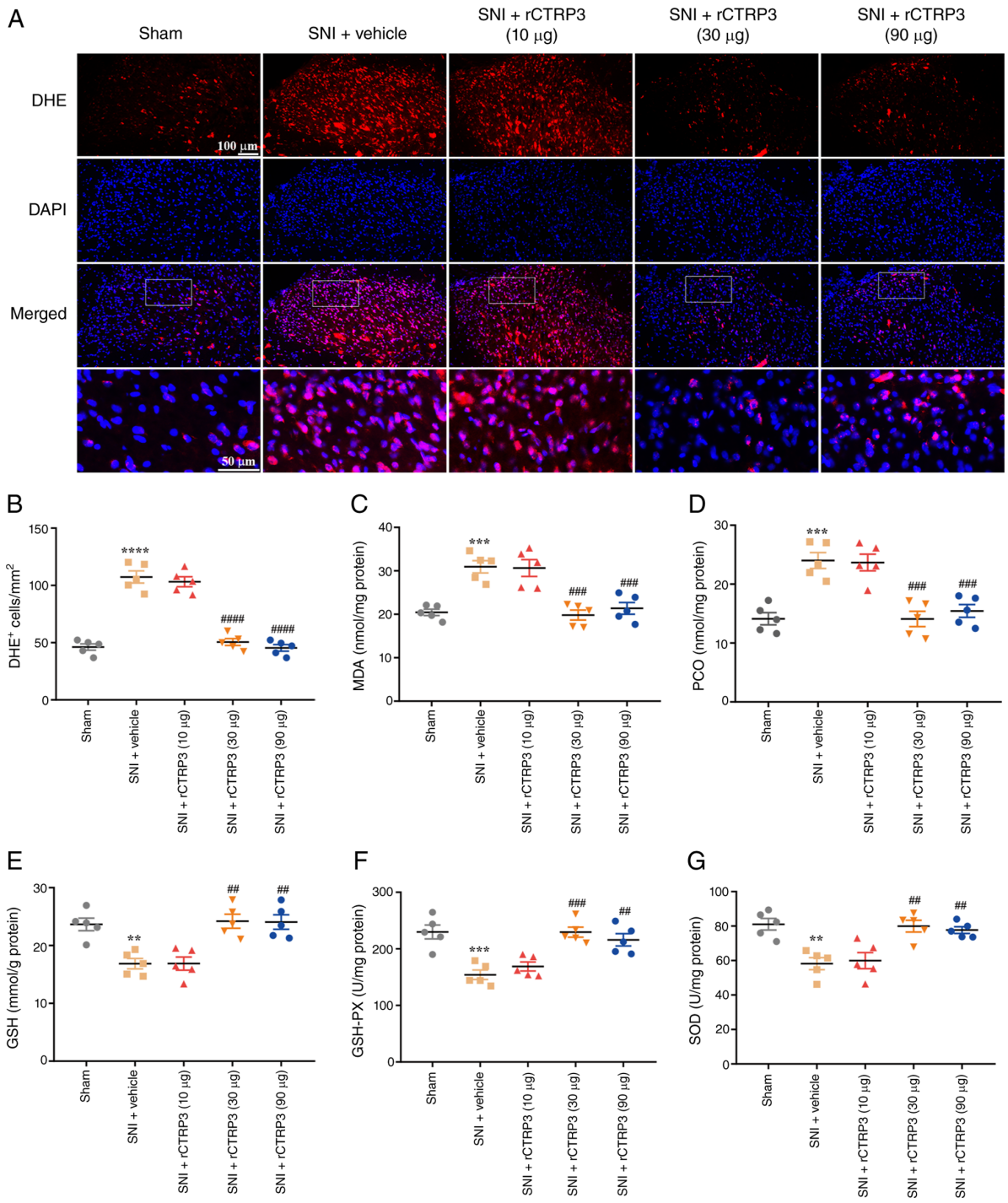

Figure 5. rCTRP3 administration attenuates SNI-induced oxidative stress in the rat spinal cord. (A and B) DHE staining showed that rCTRP3 treatment (30 and 90 μg) significantly reduced the increased number of DHE-positive cells in the spinal dorsal horn of SNI rats. (C and D) Biochemical assays revealed that SNI elevated the spinal content of MDA and PCO; intrathecal injection of rCTRP3 (30 and 90 μg) reversed this elevation. (E and F) rCTRP3 (30 and 90 μg) restored the reduced concentrations of reduced GSH and activity of GSH-PX in the spinal cord of SNI rats. (G) Administration of rCTRP3 (30 and 90 μg) reversed the decreased activity of SOD in the spinal cord of SNI rats. **P<0.01, ***P<0.001 and ****P<0.0001 vs. sham group; $^{\#\#}$P<0.01, $^{\#\#\#}$P<0.001 and $^{\#\#\#\#}$P<0.0001 vs. SNI + vehicle group; n=5 rats/group. rCTRP3, recombinant complement C1q tumor necrosis factor-related protein 3; SNI, spared nerve injury; DHE, dihydroethidium; MDA, malondialdehyde; PCO, protein carbonyl; GSH, glutathione; GSH-PX, glutathione peroxidase; SOD, superoxide dismutase.

spinal cord of SNI rats. These findings confirm that CTRP3 can alleviate SNI-induced oxidative stress in the spinal cord of rats.

SIRT1 antagonist abolishes rCTRP3-mediated amelioration of pain hypersensitivity and mitochondrial biogenesis in SNI rats. To investigate whether SIRT1 mediates the analgesic effect of rCTRP3 in SNI rats, the SIRT1 antagonist EX-527 was employed. Results demonstrated that rCTRP3 treatment restored the reduced PWT [Fig. 6A: Interaction: F (15, 216)=6.652, P<0.0001, η^2=0.3160; Time factor: F (5, 216)=44.13, P<0.0001, η^2=0.5053; Group factor: F (3, 216)=148.5, P<0.0001, η^2=0.6734] and attenuated the elevated PWCD [Fig. 6B: Interaction: F (15, 216)=7.944, P<0.0001, η^2=0.3556; Time factor: F (5, 216)=51.85,

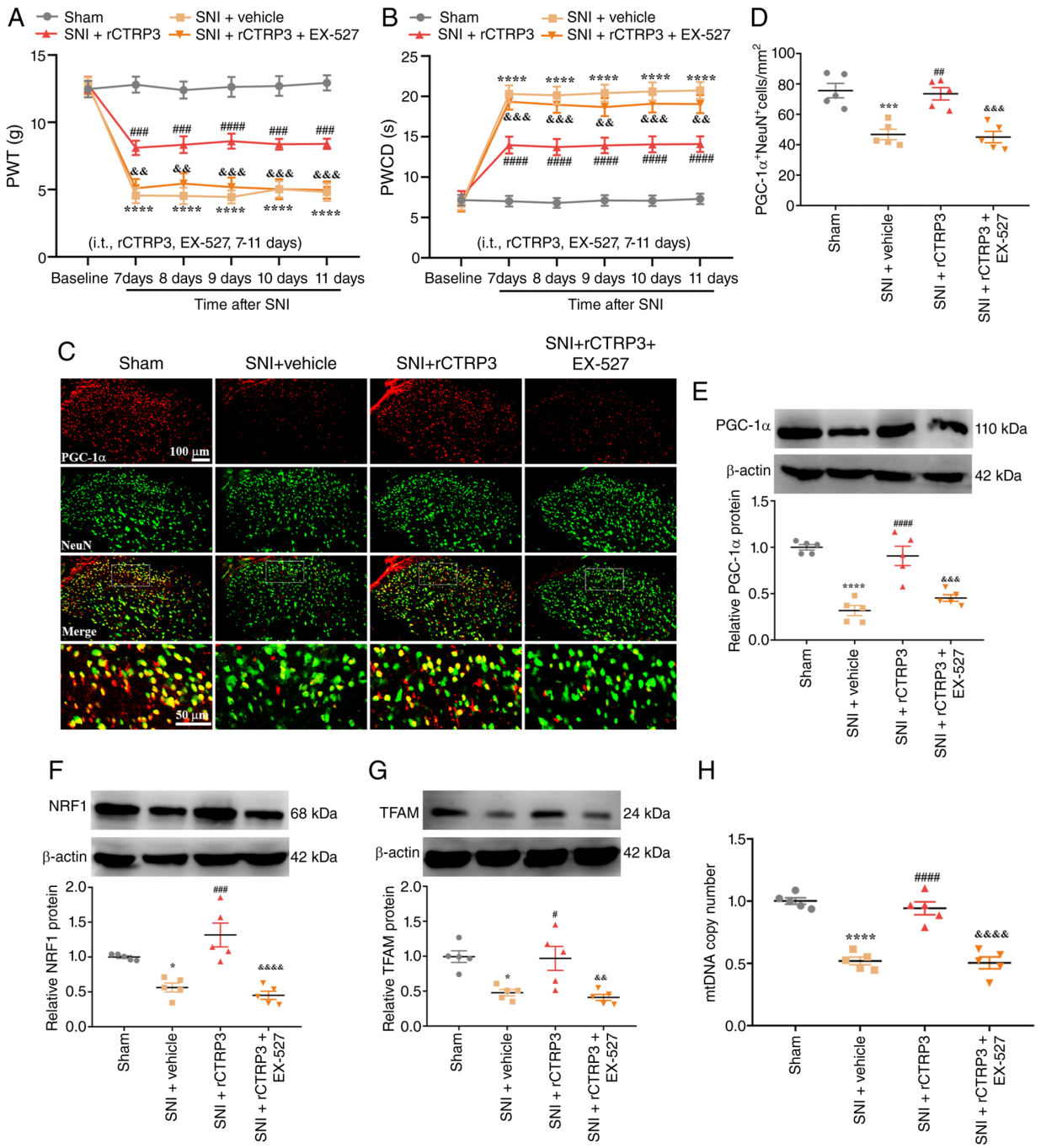

Figure 6. SIRT1 antagonist abrogates rCTRP3-mediated amelioration of pain hypersensitivity and PGC-1α-dependent mitochondrial biogenesis in SNI rats. (A and B) Intrathecal injection of EX-527 (a SIRT1 antagonist) reversed the rCTRP3-induced increases in PWT and reductions in PWCD in SNI rats. ****P<0.0001 vs. sham group; $^{###}$P<0.001 and $^{####}$P<0.0001 vs. SNI + vehicle group; $^{&&}$P<0.01 and $^{&&&}$P<0.001 vs. SNI + rCTRP3 group; n=10 rats/group. (C and D) IF staining revealed that EX-527 blocked the rCTRP3-induced upregulation of PGC-1α expression in spinal dorsal horn neurons of SNI rats. (E-G) WB analysis demonstrated that EX-527 abolished the rCTRP3-mediated elevation of PGC-1α, NRF1 and TFAM levels in the spinal cord of SNI rats. (H) Administration of rCTRP3 reversed the reduction in mtDNA copy number in SNI rats, but this protective effect was inhibited by EX-527. *P<0.05, ***P<0.001 and ****P<0.0001 vs. sham group; $^{#}$P<0.05, $^{##}$P<0.01, $^{###}$P<0.001 and $^{####}$P<0.0001 vs. SNI + vehicle group; $^{&&}$P<0.01, $^{&&&}$P<0.001 and $^{&&&&}$P<0.0001 vs. SNI + rCTRP3 group; n=5 rats/group. SIRT1, sirtuin 1; rCTRP3, recombinant complement C1q tumor necrosis factor-related protein 3; SNI, spared nerve injury; EX-527, a selective SIRT1 antagonist; PWT, paw withdrawal threshold; PWCD, paw withdrawal cold duration; IF, immunofluorescence; WB, Western blotting; PGC-1α, peroxisome proliferator-activated receptor gamma coactivator 1-alpha; NRF1, nuclear respiratory factor 1; TFAM, mitochondrial transcription factor A; mtDNA, mitochondrial DNA.

P<0.0001, η^2=0.5455; Group factor: F (3, 216)=175.3, P<0.0001, η^2=0.7088] in SNI rats; however, co-administration of EX-527 abolished this analgesic effect of rCTRP3. These data indicated that CTRP3 alleviates mechanical allodynia and cold hyperalgesia by activating spinal SIRT1 in SNI rats. Furthermore, to explore the mechanism by which CTRP3 regulates mitochondrial biogenesis, EX-527 was used in subsequent experiments. IF staining revealed that EX-527 blocked the rCTRP3-induced increase in PGC-1α expression in spinal dorsal horn neurons of SNI

rats [Fig. 6C and D: F (3, 16)=16.84, P<0.0001, η^2=0.7594]. Consistently, WB analysis identified that EX-527 abolished the rCTRP3-mediated upregulation of PGC-1α [Fig. 6E: F (3, 16)=27.96, P<0.0001, η^2=0.8398], NRF1 [Fig. 6F: F (3, 16)=17.25, P<0.0001, η^2=0.7639] and TFAM [Fig. 6G: F (3, 16)=9.562, P=0.0007, η^2=0.6419] in the spinal cord, compared with the SNI + rCTRP3 group. Additionally, rCTRP3 treatment reversed the reduction in mtDNA copy number in SNI rats, but this effect was blocked by EX-527 [Fig. 6H: F (3, 16)=44.02, P<0.0001, η^2=0.8919]. These results confirm that CTRP3 alleviates mechanical allodynia and cold hyperalgesia and promotes PGC-1α-mediated mitochondrial biogenesis in the spinal cord of SNI rats through SIRT1 activation.

SIRT1 antagonist blocks rCTRP3-induced enhancement of UPR^{mt} in SNI rats. To investigate the mechanism by which CTRP3 regulates the UPR^{mt}, the SIRT1 antagonist EX-527 was utilized in the present study. IF staining results revealed that EX-527 inhibited the rCTRP3-induced increase in ATF5 expression in spinal dorsal horn neurons of SNI rats [Fig. 7A and B: F (3, 16)=15.36, P<0.0001, η^2=0.7423]. Consistently, RT-qPCR analysis demonstrated that EX-527 abolished the rCTRP3-mediated upregulation of ATF5 [Fig. 7C: F (3, 16)=24.98, P<0.0001, η^2=0.8240], ClpP [Fig. 7D: F (3, 16)=14.60, P<0.0001; η^2=0.7324], Hsp60 [Fig. 7E: F (3, 16)=17.52, P=0.0007, η^2=0.7666] and LonP1 [Fig. 7F: F (3, 16)=15.18, P<0.0001, η^2=0.7400] in the spinal cord, relative to the SNI + rCTRP3 group. These findings demonstrate that CTRP3 promotes ATF5-mediated UPR^{mt} in the spinal cord of SNI rats through SIRT1 activation.

SIRT1 inhibitor abolishes rCTRP3-mediated alleviation of mitochondrial dysfunction and oxidative stress in SNI rats. Moreover, the beneficial effects of rCTRP3 on restoring MMP [F (3, 16)=20.21, P<0.0001, η^2=0.7912] and ATP production [F (3, 16)=12.61, P=0.0002, η^2=0.7028] were completely abolished by pretreatment with the SIRT1 inhibitor EX-527 (Fig. S2A-C), indicating that SIRT1 activity is essential for rCTRP3 to maintain mitochondrial membrane integrity and energy production. As demonstrated in Fig. 8A and B [F (3, 16)=58.50, P<0.0001, η^2=0.9164], DHE staining revealed that compared with the SNI + rCTRP3 group, treatment with EX-527 reversed the rCTRP3-induced reduction in the number of DHE-positive cells in the spinal cord of SNI rats. Furthermore, biochemical assay results demonstrated that EX-527 abolished the rCTRP3-mediated downregulation of oxidative damage markers, including MDA [Fig. 8C: F (3, 16)=18.93, P<0.0001, η^2=0.7802] and PCO [Fig. 8D: F (3, 16)=17.45, P<0.0001, η^2=0.7659] in the spinal cord of SNI rats. Notably, while rCTRP3 increased the level of GSH [Fig. 8E: F (3, 16)=9.383, P=0.0008, η^2=0.6376] and enhanced the activity of antioxidant enzymes such as GSH-PX [Fig. 8F: F (3, 16)=12.27, P=0.0002, η^2=0.6970] and SOD [Fig. 8G: F (3, 16)=12.34, P=0.0002, η^2=0.6983] in the spinal cord of SNI rats, these beneficial effects were reversed by the SIRT1 antagonist. These findings confirm that CTRP3 mitigates spinal oxidative stress in SNI rats through SIRT1 activation.

PGC-1α siRNA abolishes rCTRP3-mediated amelioration of pain hypersensitivity, mitochondrial biogenesis and ATF5-dependent UPR^{mt} in SNI rats. To establish whether PGC-1α serves as a critical downstream mediator of rCTRP3-induced analgesia in SNI rats, PGC-1α expression in the spinal cord was specifically silenced using siRNA. RT-qPCR analysis confirmed that PGC-1α siRNA transfection induced significant downregulation of PGC-1α mRNA in PC12 cells *in vitro* without additional stimulation [Fig. 9A: t (8)=6.717, P=0.0002, η^2=0.8494]. Consistently, intrathecal injection of PGC-1α siRNA also significantly inhibited the endogenous transcription of spinal PGC-1α in SNI rats compared with the negative control siRNA group [Fig. 9B: t (8)=6.654, P=0.0002, η^2=0.8470]. Subsequent behavioral testing demonstrated that intrathecal administration of rCTRP3 significantly elevated the reduced PWT and reduced the prolonged PWCD in SNI-operated rats; however, these analgesic effects were completely abrogated by co-delivery of PGC-1α siRNA [Fig. 9B and C; Fig. 9B: Interaction: F (20, 270)=6.262, P<0.0001, η^2=0.3169; Time factor: F (5, 270)=62.06, P<0.0001, η^2=0.5347; Group factor: F (4, 270)=143.9, P<0.0001, η^2=0.6807; Fig. 9C: Interaction: F (20, 270)=6.418, P<0.0001, η^2=0.3222; Time factor: F (5, 270)=80.32, P<0.0001, η^2=0.5980; Group factor: F (4, 270)=168.2, P<0.0001, η^2=0.7137]. These results indicate that PGC-1α activation is essential for rCTRP3 to alleviate mechanical allodynia and cold hyperalgesia in the context of neuropathic pain.

To further clarify the regulatory role of PGC-1α in mitochondrial biogenesis triggered by rCTRP3, IF staining and WB analysis were performed. IF staining revealed that PGC-1α siRNA significantly blocked the rCTRP3-mediated upregulation of PGC-1α in neurons of the spinal dorsal horn [Fig. 10A and B: F (4, 20)=14.12, P<0.0001, η^2=0.7385]. In line with this observation, WB analysis demonstrated that PGC-1α silencing abolished the rCTRP3-induced increases in PGC-1α [F (4, 20)=7.979, P=0.0005, η^2=0.6148], NRF1 [F (4, 20)=38.50, P<0.0001, η^2=0.8850] and TFAM [F (4, 20)=19.60, P<0.0001, η^2=0.7967] protein levels in the spinal cord, as compared with the SNI + rCTRP3 group (Fig. 10C-E). Moreover, rCTRP3 treatment effectively reversed the SNI-induced reduction in mtDNA copy number, and this beneficial effect was also negated by PGC-1α siRNA intervention [Fig. 10F: F (4, 20)=16.59, P<0.0001, η^2=0.7684].

Notably, it was further explored whether PGC-1α could modulate ATF5-mediated UPR^{mt} during rCTRP3 treatment. IF staining showed that PGC-1α siRNA significantly inhibited the rCTRP3-evoked upregulation of ATF5 in spinal dorsal horn neurons [Fig. S3A and B: F (4, 20)=15.48, P<0.0001, η^2=0.7558]. Consistently, RT-qPCR analysis revealed that silencing PGC-1α completely reversed the rCTRP3-mediated enhancement of ATF5 [F (4, 20)=13.22, P<0.0001, η^2=0.7256], ClpP [F (4, 20)=14.29, P<0.0001, η^2=0.7408], Hsp60 [F (4, 20)=13.33, P<0.0001, η^2=0.7273] and LonP1 [F (4, 20)=14.17, P<0.0001, η^2=0.7391] mRNA expression in the spinal cord (Fig. S3C-F). Collectively, these findings demonstrate that PGC-1α functions as a key molecular hub that enables rCTRP3 to simultaneously promote mitochondrial biogenesis and ATF5-dependent UPR^{mt}, ultimately mitigating neuropathic pain hypersensitivity.

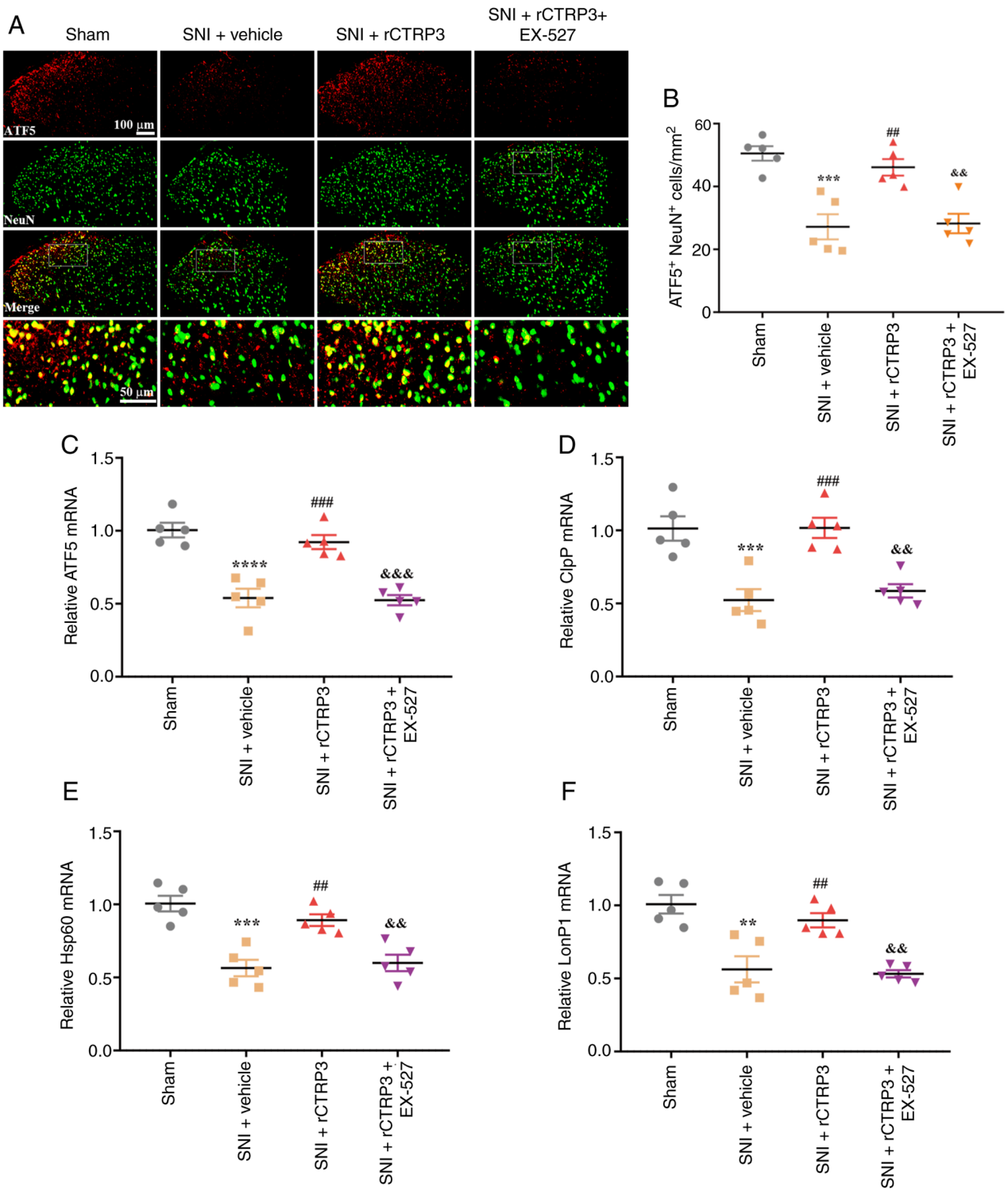

Figure 7. SIRT1 antagonist blocks rCTRP3-induced enhancement of ATF5-mediated UPR^{mt} in SNI rats. (A and B) IF staining results showed that EX-527 inhibited the rCTRP3-induced upregulation of ATF5 expression in spinal dorsal horn neurons of SNI rats. (C-F) RT-qPCR analysis demonstrated that EX-527 abolished the rCTRP3-mediated elevation of ATF5, ClpP, Hsp60 and LonP1 expression in the spinal cord, compared with the SNI + rCTRP3 group. **P<0.01, ***P<0.001 and ****P<0.0001 vs. sham group; $^{\#\#}$P<0.01 and $^{\#\#\#}$P<0.001 vs. SNI + vehicle group; $^{\&\&}$P<0.01 and $^{\&\&\&}$P<0.001 vs. SNI + rCTRP3 group; n=5 rats/group. SIRT1, sirtuin 1; rCTRP3, recombinant complement C1q tumor necrosis factor-related protein 3; SNI, spared nerve injury; EX-527, selective SIRT1 inhibitor; IF, immunofluorescence; RT-qPCR, reverse transcription-quantitative polymerase chain reaction; ATF5, activating transcription factor 5; UPR^{mt}, mitochondrial unfolded protein response; ClpP, caseinolytic mitochondrial matrix peptidase proteolytic subunit; Hsp60, heat shock protein 60; LonP1, Lon protease 1.

PGC-1α siRNA blocks rCTRP3-induced attenuation of spinal mitochondrial dysfunction and oxidative stress in SNI rats. Similarly, silencing PGC-1α via siRNA also blocked the rCTRP3-induced restoration of MMP [F (4, 20)=24.04, P<0.0001, η^2=0.8278] and ATP content [F (4, 20)=15.84, P<0.0001, η^2=0.7601] in the spinal cord of SNI rats (Fig. S4A-C), supporting that PGC-1α-dependent mitochondrial biogenesis is required for rCTRP3 to sustain normal mitochondrial function.

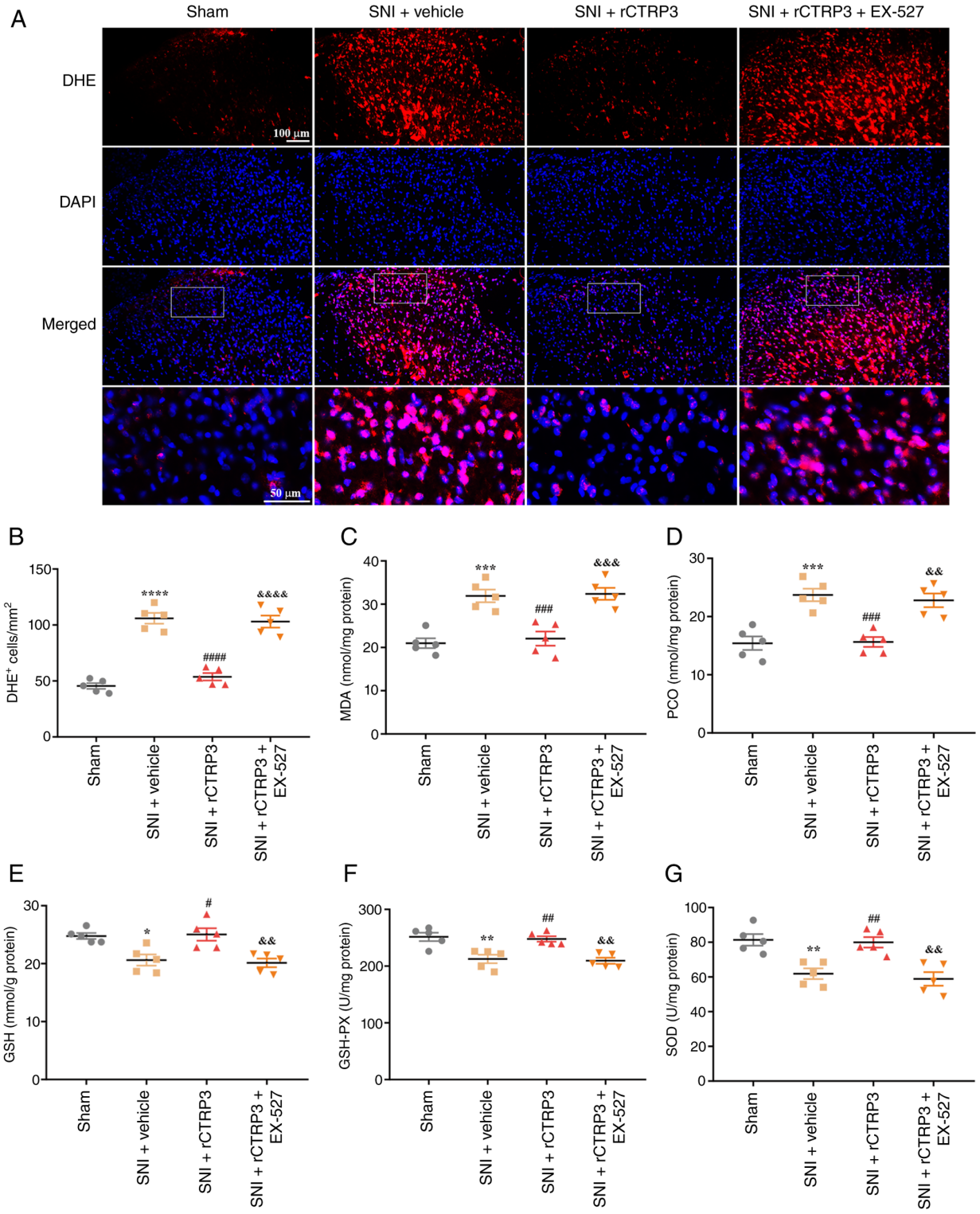

Figure 8. SIRT1 inhibitor abrogates rCTRP3-induced attenuation of spinal oxidative stress in SNI rats. (A and B) DHE staining revealed that, compared with the SNI + rCTRP3 group, EX-527 treatment reversed the rCTRP3-induced decrease in the number of DHE-positive cells in the spinal cord of SNI rats. (C and D) Biochemical assay results demonstrated that EX-527 eliminated the rCTRP3-mediated reduction in spinal levels of MDA and PCO in SNI rats. (E-G) rCTRP3 treatment increased the spinal level of reduced GSH and enhanced the activity of GSH-PX and SOD in SNI rats; however, these protective effects were counteracted by the SIRT1 antagonist (EX-527). *P<0.05, **P<0.01, ***P<0.001 and ****P<0.0001 vs. sham group; $^{\#}$P<0.05, $^{\#\#}$P<0.01, $^{\#\#\#}$P<0.001 and $^{\#\#\#\#}$P<0.0001 vs. SNI + vehicle group; $^{\&\&}$P<0.01, $^{\&\&\&}$P<0.001 and $^{\&\&\&\&}$P<0.0001 vs. SNI + rCTRP3 group; n=5 rats/group. SIRT1, sirtuin 1; rCTRP3, recombinant complement C1q tumor necrosis factor-related protein 3; SNI, spared nerve injury; EX-527, a selective SIRT1 inhibitor; DHE, dihydroethidium; MDA, malondialdehyde; PCO, protein carbonyl; GSH, glutathione; GSH-PX, glutathione peroxidase; SOD, superoxide dismutase.

As depicted in Fig. 11A and B [F (4, 20)=52.53, P<0.0001, η^2=0.9131], DHE staining analysis showed that compared with the SNI + rCTRP3 group, administration of PGC-1α siRNA counteracted the rCTRP3-induced decrease in the number of DHE-positive cells in the spinal cord of SNI rats. In addition, biochemical assay data revealed that PGC-1α siRNA eliminated

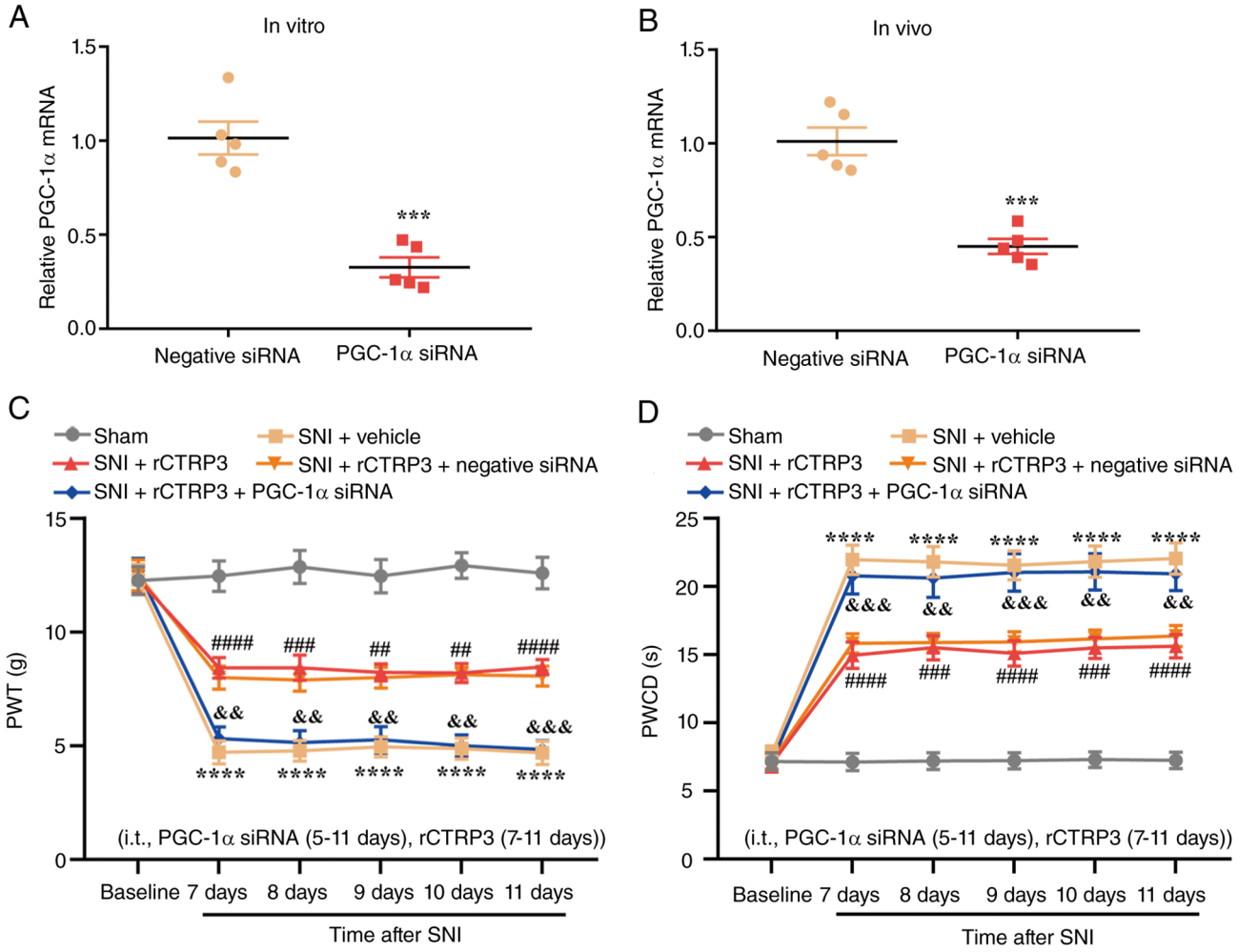

Figure 9. PGC-1α siRNA abrogates rCTRP3-mediated alleviation of pain hypersensitivity in SNI rats. (A) RT-qPCR analysis confirmed that PGC-1α siRNA transfection induced significant downregulation of PGC-1α mRNA in PC12 cells. ***P<0.001 vs. negative siRNA group; n=5. (B) RT-qPCR results verified that PGC-1α siRNA efficiently suppressed PGC-1α expression in the spinal cord. ***P<0.001 vs. negative siRNA group; n=5 rats/group. (C and D) Behavioral assessments showed that rCTRP3 treatment increased PWT and reduced PWCD in SNI rats; however, co-administration of PGC-1α siRNA reversed this analgesic effect of rCTRP3. ****P<0.0001 vs. sham group; $^{\#\#}$P<0.01, $^{\#\#\#}$P<0.001 and $^{\#\#\#\#}$P<0.0001 vs. SNI + vehicle group; $^{\&\&}$P<0.01 and $^{\&\&\&}$P<0.001 vs. SNI + rCTRP3 group; n=10 rats/group. PGC-1α, peroxisome proliferator-activated receptor gamma coactivator 1-alpha; siRNA, small interfering RNA; rCTRP3, recombinant complement C1q tumor necrosis factor-related protein 3; SNI, spared nerve injury; RT-qPCR, reverse transcription-quantitative polymerase chain reaction; PWT, paw withdrawal threshold; PWCD, paw withdrawal cold duration.

the rCTRP3-driven downregulation of oxidative damage indicators, specifically MDA [Fig. 11C: F (4, 20)=18.60, P<0.0001, η^2=0.7881] and PCO [Fig. 11D: F (4, 20)=18.20, P<0.0001, η^2=0.7845] in the spinal cord of SNI rats. Of note, although rCTRP3 elevated the level of GSH [Fig. 11E: F (4, 20)=14.86, P<0.0001, η^2=0.7483] and improved the activity of antioxidant enzymes including GSH-PX [Fig. 11F: F (4, 20)=11.54, P<0.0001, η^2=0.6977] and SOD [Fig. 11G: F (4, 20)=22.86, P<0.0001, η^2=0.8205] in the spinal cord of SNI rats, these favorable changes were reversed by PGC-1α siRNA intervention. These results indicate that CTRP3 alleviates spinal oxidative stress in SNI rats through the activation of PGC-1α.

ATF5 siRNA reverses rCTRP3-mediated attenuation of pain hypersensitivity, UPR^{mt} activation and PGC-1α-dependent mitochondrial biogenesis in SNI rats. To define the functional contribution of ATF5 to rCTRP3-evoked analgesic effects, siRNA was used to specifically knock down ATF5 expression in the spinal cord of SNI rats. RT-qPCR analysis confirmed that ATF5 siRNA transfection induced significant downregulation of ATF5 mRNA in PC12 cells *in vitro* without additional stimulation [Fig. 12A, t (8)=9.359, P<0.0001, η^2=0.9163]. Consistently, intrathecal injection of ATF5 siRNA also significantly inhibited the endogenous transcription of spinal ATF5 in SNI rats compared with the negative control siRNA group [Fig. 12B, t (8)=6.954, P=0.0001, η^2=0.8581]. Behavioral assessments revealed that rCTRP3 treatment significantly restored PWT and shortened PWCD in SNI rats, whereas combined administration of ATF5 siRNA fully abolished these pain-relieving effects [Fig. 12B and C; Fig. 12B: Interaction: F (20, 270)=4.874, P<0.0001, η^2=0.2652; Time factor: F (5, 270)=49.97, P<0.0001, η^2 =0.4807; Group factor: F (4, 270)=121.0, P<0.0001, η^2=0.6419; Fig. 12C: Interaction: F (20, 270)=7.286, P<0.0001, η^2=0.3505; Time factor: F (5, 270)=91.13, P<0.0001, η^2=0.6279; Group factor: F (4, 270)=196.1, P<0.0001, η^2=0.7439]. These data confirm that ATF5 activation is required for rCTRP3 to exert its anti-nociceptive actions in neuropathic pain.

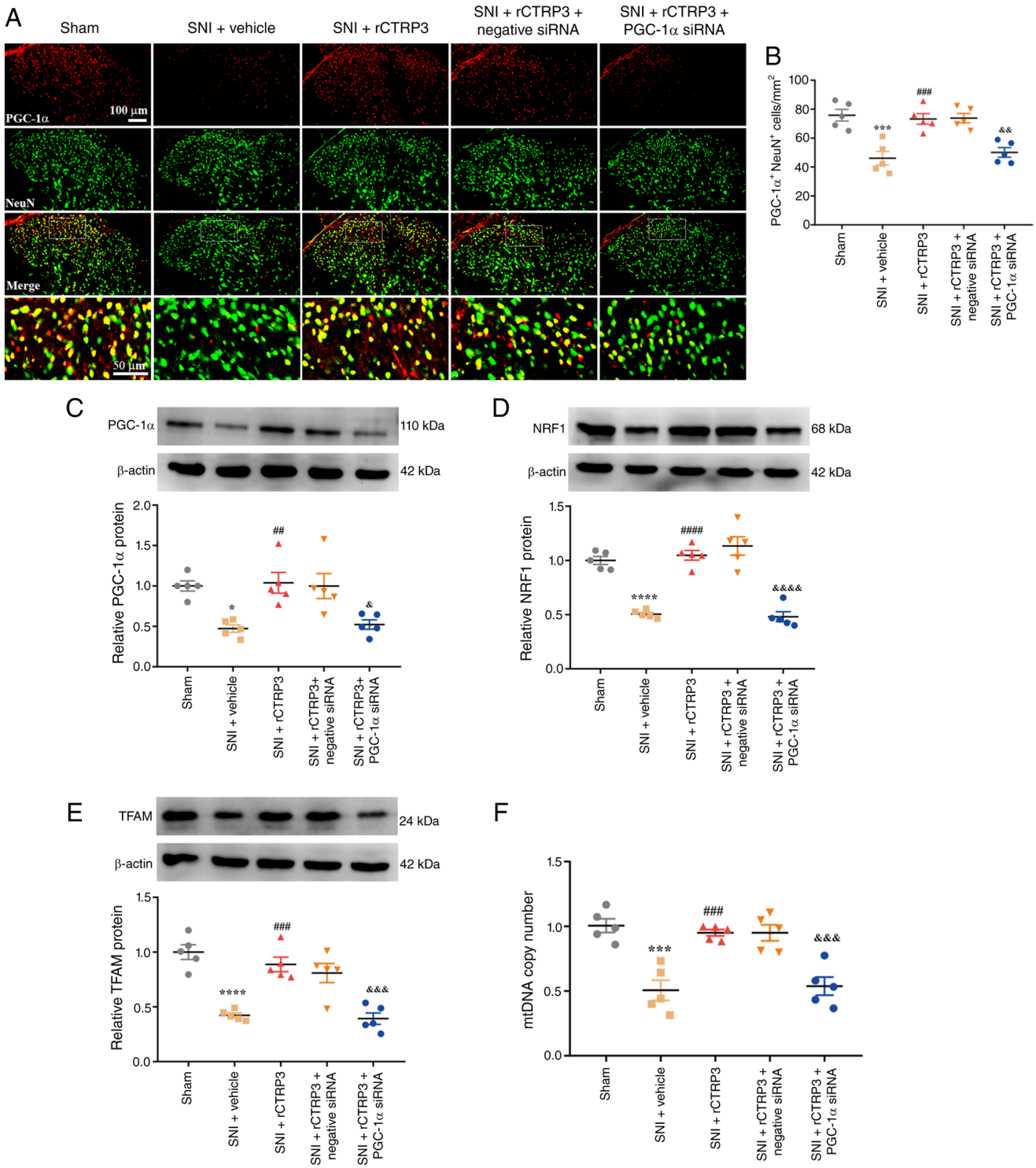

Figure 10. PGC-1α siRNA abrogates rCTRP3-mediated enhancement of mitochondrial biogenesis in SNI rats. (A and B) IF staining revealed that PGC-1α siRNA blocked the rCTRP3-induced upregulation of PGC-1α expression in spinal dorsal horn neurons of SNI rats. (C-E) WB analysis demonstrated that PGC-1α siRNA eliminated the rCTRP3-mediated elevation of PGC-1α, NRF1, and TFAM levels in the spinal cord, compared with the SNI + rCTRP3 group. (F) rCTRP3 treatment reversed the reduction in mtDNA copy number in SNI rats, and this regulatory effect was inhibited by PGC-1α siRNA. *P<0.05, ***P<0.001 and ****P<0.0001 vs. sham group; $^{\#\#}$P<0.01, $^{\#\#\#}$P<0.001 and $^{\#\#\#\#}$P<0.0001 vs. SNI + vehicle group; $^{\&}$P<0.05, $^{\&\&}$P<0.01, $^{\&\&\&}$P<0.001 and $^{\&\&\&\&}$P<0.0001 vs. SNI + rCTRP3 group; n=5 rats/group. PGC-1α, peroxisome proliferator-activated receptor gamma coactivator 1-alpha; siRNA, small interfering RNA; rCTRP3, recombinant complement C1q tumor necrosis factor-related protein 3; SNI, spared nerve injury; IF, immunofluorescence; WB, Western blotting; NRF1, nuclear respiratory factor 1; TFAM, mitochondrial transcription factor A; mtDNA, mitochondrial DNA.

The impact of ATF5 silencing on rCTRP3-mediated regulation of UPR^{mt} was next examined. IF staining showed that ATF5 siRNA significantly suppressed the rCTRP3-induced elevation of ATF5 in neurons of the spinal dorsal horn [Fig. 13A and B: F (4, 20)=11.67, P<0.0001, η^2=0.7001]. Correspondingly, RT-qPCR analysis demonstrated that ATF5 knockdown abolished the rCTRP3-mediated upregulation of ATF5 [F (4, 20)=14.71, P<0.0001, η^2=0.7464], ClpP

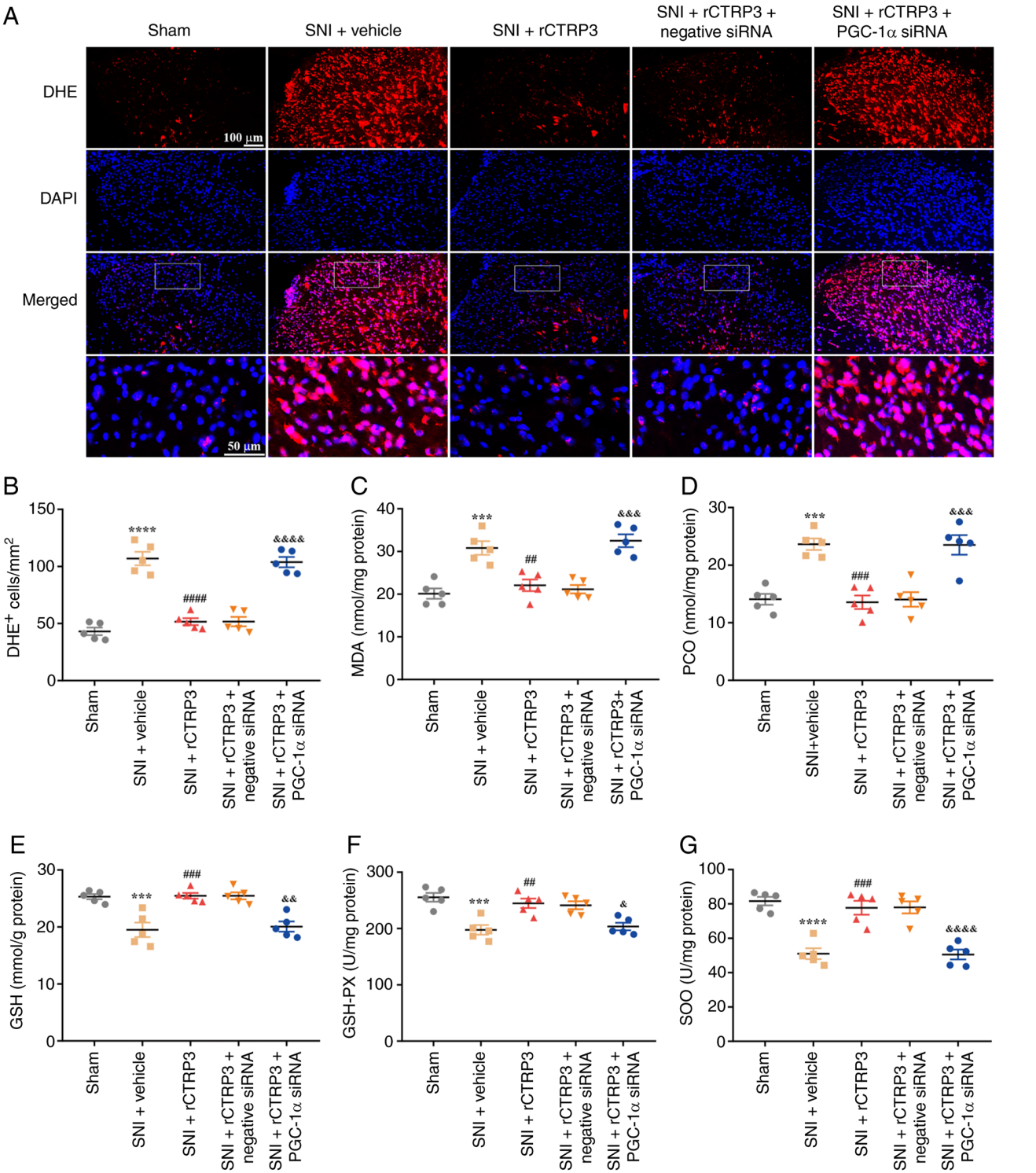

Figure 11. PGC-1α siRNA blocks rCTRP3-induced reduction of spinal oxidative stress in SNI rats. (A and B) DHE staining analysis showed that compared with the SNI + rCTRP3 group, administration of PGC-1α siRNA reversed the rCTRP3-induced decrease in the number of DHE-positive cells in the spinal cord of SNI rats. (C and D) Biochemical assay results revealed that PGC-1α siRNA abolished the rCTRP3-mediated downregulation of MDA and PCO, in the spinal cord of SNI rats. (E-G) Administration of rCTRP3 increased the level of reduced GSH and enhanced the activity of GSH-PX and SOD in the spinal cord of SNI rats, but these beneficial changes were counteracted by PGC-1α siRNA intervention. ***P<0.001 and ****P<0.0001 vs. sham group; $^{\#\#}$P<0.01, $^{\#\#\#}$P<0.001 and $^{\#\#\#\#}$P<0.0001 vs. SNI + vehicle group; $^{\&}$P<0.05, $^{\&\&}$P<0.01, $^{\&\&\&}$P<0.001 and $^{\&\&\&\&}$P<0.0001 vs. SNI + rCTRP3 group; n=5 rats/group. PGC-1α, peroxisome proliferator-activated receptor gamma coactivator 1-alpha; siRNA, small interfering RNA; rCTRP3, recombinant complement C1q tumor necrosis factor-related protein 3; SNI, spared nerve injury; DHE, dihydroethidium; MDA, malondialdehyde; PCO, protein carbonyl; GSH, glutathione; GSH-PX, glutathione peroxidase; SOD, superoxide dismutase.

[F (4, 20)=14.10, P<0.0001, η^2=0.7383], Hsp60 [F (4, 20)=8.704, P=0.0003, η^2=0.6351] and LonP1 [F (4, 20)=18.67, P<0.0001, η^2=0.7888] transcripts in the spinal cord, relative to the SNI + rCTRP3 group (Fig. 13C-F). These results confirm that ATF5 is indispensable for rCTRP3 to trigger the UPR^{mt} in the spinal cord after nerve injury.

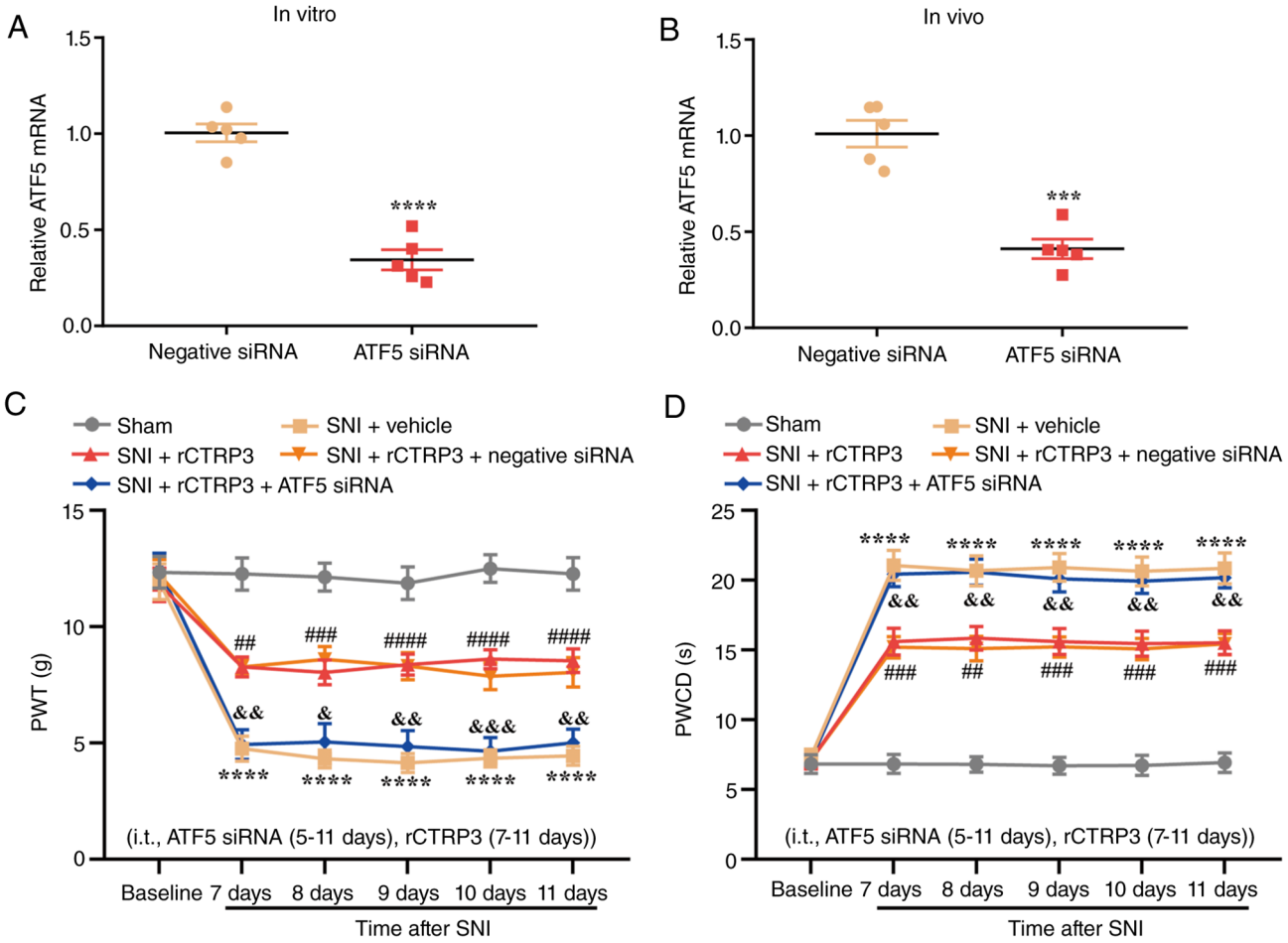

Figure 12. ATF5 siRNA abrogates rCTRP3-mediated alleviation of pain hypersensitivity in SNI rats. (A) RT-qPCR analysis confirmed that ATF5 siRNA transfection induced significant downregulation of ATF5 mRNA in PC12 cells. ****P<0.0001 vs. negative siRNA group; n=5. (B) RT-qPCR results confirmed that ATF5 siRNA effectively inhibited ATF5 expression in the spinal cord. ***P<0.001 vs. negative siRNA group; n=5 rats/group. (C and D) Behavioral assessments demonstrated that rCTRP3 treatment elevated PWT and downregulated PWCD in SNI rats; however, co-administration of ATF5 siRNA reversed this analgesic effect of rCTRP3. ****P<0.0001 vs. sham group; $^{\#\#}$P<0.01, $^{\#\#\#}$P<0.001 and $^{\#\#\#\#}$P<0.0001 vs. SNI + vehicle group; $^{\&}$P<0.05, $^{\&\&}$P<0.01 and $^{\&\&\&}$P<0.001 vs. SNI + rCTRP3 group; n=10 rats/group. ATF5, activating transcription factor 5; siRNA, small interfering RNA; rCTRP3, recombinant complement C1q tumor necrosis factor-related protein; SNI, spared nerve injury; RT-qPCR, reverse transcription-quantitative polymerase chain reaction; PWT, paw withdrawal threshold; PWCD, paw withdrawal cold duration.

To test whether ATF5 also modulates mitochondrial biogenesis downstream of rCTRP3, key molecules involved in this process were assessed. IF staining revealed that ATF5 siRNA significantly inhibited the rCTRP3-mediated increase in PGC-1α expression in spinal dorsal horn neurons [Fig. S5A and B: $F(4, 20)=14.20$, $P<0.0001$, $\eta^2=0.7395$]. In agreement, WB analysis showed that ATF5 silencing significantly reversed the rCTRP3-induced upregulation of PGC-1α [$F(4, 20)=15.32$, $P<0.0001$, $\eta^2=0.7539$], NRF1 [$F(4, 20)=11.57$, $P<0.0001$, $\eta^2=0.6982$] and TFAM [$F(4, 20)=15.69$, $P<0.0001$, $\eta^2=0.7583$] proteins in the spinal cord (Fig. S5C-E). Taken together, these results demonstrate that ATF5 acts as a critical downstream effector that supports rCTRP3-induced UPR^{mt} and cooperatively enhances PGC-1α-dependent mitochondrial biogenesis, thereby contributing to the alleviation of neuropathic pain.

ATF5 siRNA abrogates rCTRP3-mediated restoration of mitochondrial function and reduction of oxidative stress in SNI rats. In parallel, ATF5 siRNA eliminated the rCTRP3-induced restoration of MMP [$F(4, 20)=12.34$, $P<0.0001$, $\eta^2=0.7116$] and ATP production [$F(4, 20)=16.38$, $P<0.0001$, $\eta^2=0.7661$] (Fig. S6A-C), demonstrating that ATF5-mediated UPR^{mt} also contributes to the improved mitochondrial bioenergetics induced by rCTRP3. DHE staining analysis indicated that compared with the SNI + rCTRP3 group, administration of ATF5 siRNA reversed the rCTRP3-induced decrease in the number of DHE-positive cells in the spinal cord of SNI rats [Fig. 14A and B: $F(4, 20)=65.07$, $P<0.0001$, $\eta^2=0.9286$]. Moreover, biochemical assay results revealed that ATF5 siRNA eliminated the rCTRP3-mediated downregulation of oxidative damage markers, including MDA [Fig. 14C: $F(4, 20)=17.76$, $P<0.0001$, $\eta^2=0.7803$] and PCO [Fig. 14D: $F(4, 20)=9.924$, $P=0.0001$, $\eta^2=0.6650$] in the spinal cord of SNI rats. Notably, while rCTRP3 increased the level of GSH [Fig. 14E: $F(4, 20)=10.71$, $P<0.0001$, $\eta^2=0.6818$] and enhanced the activity of antioxidant enzymes such as GSH-PX [Fig. 14F: $F(4, 20)=13.68$, $P<0.0001$, $\eta^2=0.7323$] and SOD [Fig. 14G: $F(4, 20)=18.68$, $P<0.0001$, $\eta^2=0.7888$] in the spinal cord of SNI rats, these beneficial changes were counteracted by ATF5 siRNA intervention. These results indicate that CTRP3 mitigates spinal oxidative stress in SNI rats through ATF5 activation.

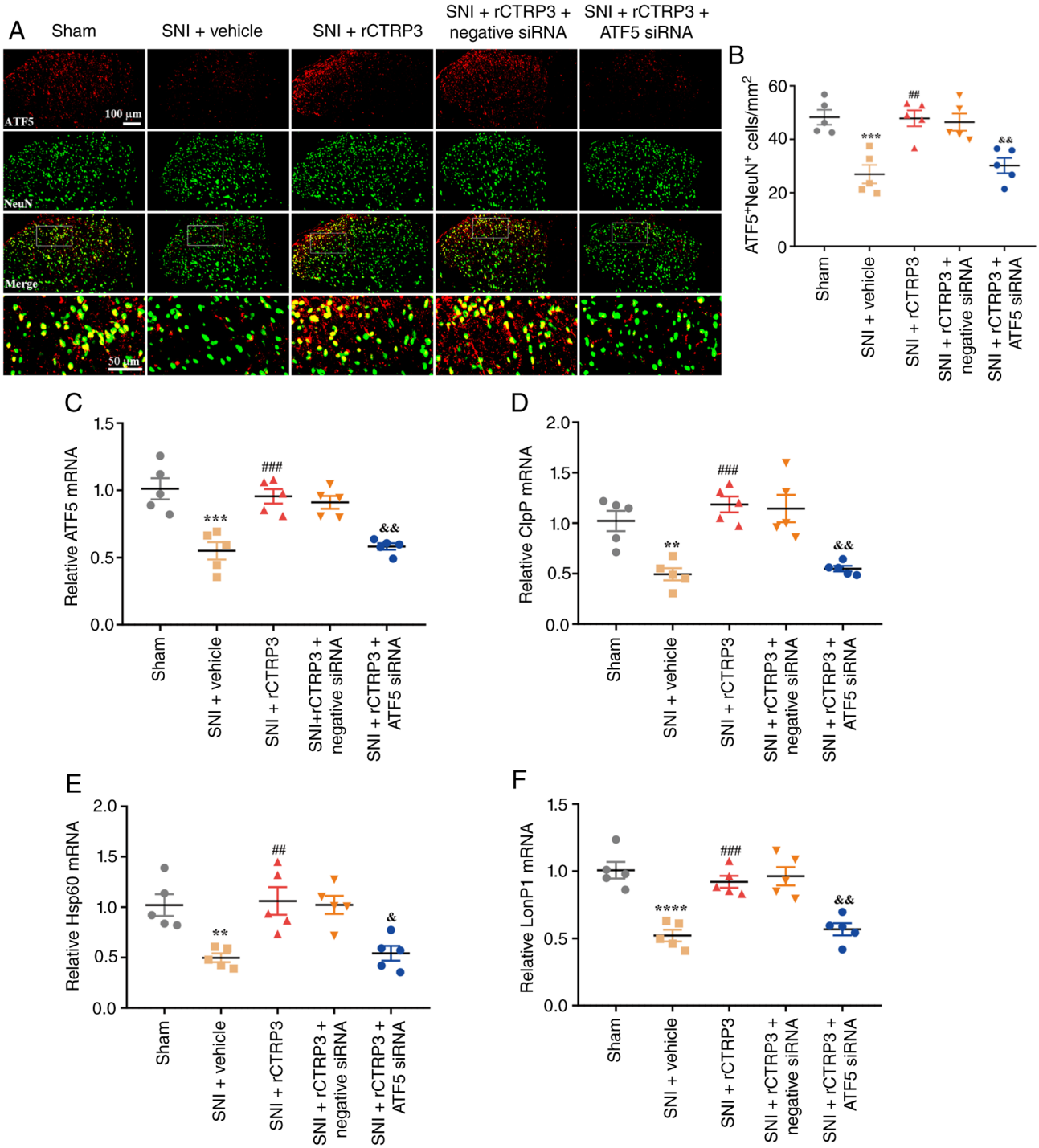

Figure 13. ATF5 siRNA abrogates rCTRP3-mediated enhancement of UPR^{mt} in SNI rats. (A and B) IF staining revealed that ATF5 siRNA inhibited the rCTRP3-induced upregulation of ATF5 expression in spinal dorsal horn neurons of SNI rats. (C-F) RT-qPCR analysis demonstrated that ATF5 siRNA eliminated the rCTRP3-mediated elevation in the expression levels of ATF5, ClpP, Hsp60 and LonP1 in the spinal cord, relative to the SNI + rCTRP3 group. **P<0.01, ***P<0.001 and ****P<0.0001 vs. sham group; $^{\#\#}$P<0.01 and $^{\#\#\#}$P<0.001 vs. SNI + vehicle group; $^{\&}$P<0.05 and $^{\&\&}$P<0.01 vs. SNI + rCTRP3 group; n=5 rats/group. ATF5, activating transcription factor 5; siRNA, small interfering RNA; rCTRP3, recombinant complement C1q tumor necrosis factor-related protein; UPR^{mt}, mitochondrial unfolded protein response; SNI, spared nerve injury; IF, immunofluorescence; RT-qPCR, reverse transcription-quantitative polymerase chain reaction; ClpP, caseinolytic mitochondrial matrix peptidase proteolytic subunit; Hsp60, heat shock protein 60; LonP1, Lon protease 1.

Discussion

In the present study, the effects of CTRP3 on neuropathic pain, mitochondrial biogenesis, and UPR^{mt}, as well as the underlying mechanisms, were investigated using a male rat model of SNI. The results showed the following: i) SNI significantly downregulated CTRP3 expression in spinal neurons; ii) intrathecal delivery of rCTRP3 relieved mechanical allodynia and cold hyperalgesia in rats with SNI; iii) rCTRP3 intervention promoted PGC-1α-dependent mitochondrial biogenesis, ATF5-initiated UPR^{mt}, and reduced oxidative stress in the spinal cord; iv) pharmacological suppression

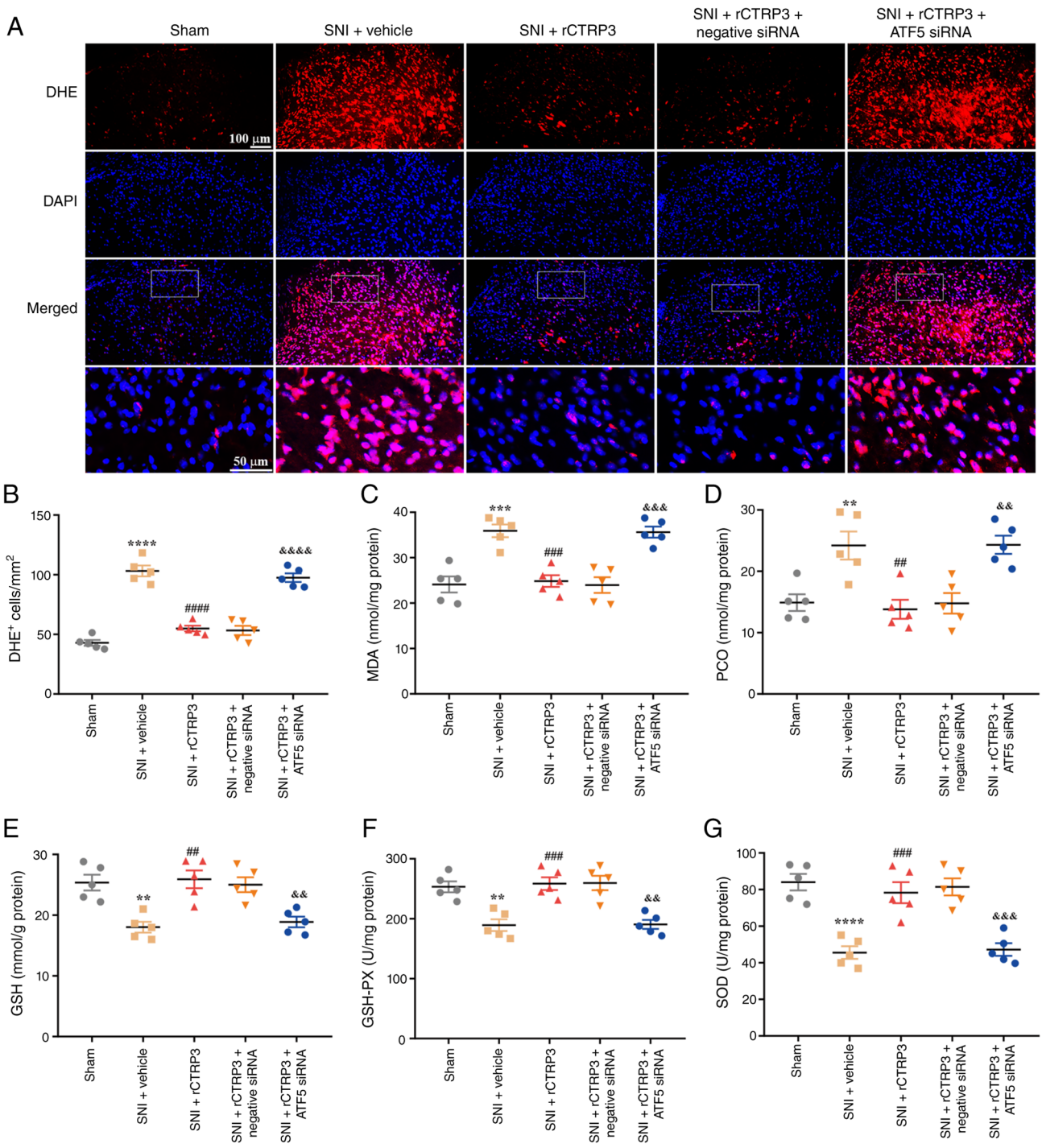

Figure 14. ATF5 siRNA abrogates rCTRP3-induced reduction of spinal oxidative stress in SNI rats. (A and B) DHE staining analysis indicated that compared with the SNI + rCTRP3 group, administration of ATF5 siRNA counteracted the rCTRP3-induced decrease in the number of DHE-positive cells in the spinal cord of SNI rats. (C and D) Biochemical assay data revealed that ATF5 siRNA abolished the rCTRP3-mediated downregulation of MDA and PCO in the spinal cord of SNI rats. (E-G) rCTRP3 treatment increased the level of reduced GSH, and enhanced the activity of GSH-PX and SOD in the spinal cord of SNI rats, but these favorable changes were reversed by ATF5 siRNA intervention. **P<0.01, ***P<0.001 and ****P<0.0001 vs. sham group; $^{\#\#}$P<0.01, $^{\#\#\#}$P<0.001 and $^{\#\#\#\#}$P<0.0001 vs. SNI + vehicle group; $^{\&\&}$P<0.01, $^{\&\&\&}$P<0.001 and $^{\&\&\&\&}$P<0.0001 vs. SNI + rCTRP3 group; n=5 rats/group. ATF5, activating transcription factor 5; siRNA, small interfering RNA; rCTRP3, recombinant complement C1q tumor necrosis factor-related protein; SNI, spared nerve injury; DHE, dihydroethidium; MDA, malondialdehyde; PCO, protein carbonyl; GSH, glutathione; GSH-PX, glutathione peroxidase; SOD, superoxide dismutase.

of SIRT1 using EX-527, and siRNA-induced knockdown of PGC-1α or ATF-5, both reversed rCTRP3's effects on pain hypersensitivity, mitochondrial biogenesis, UPR^{mt} and oxidative stress in the spinal cord. The present research reveals that CTRP3 alleviates mechanical allodynia and cold hyperalgesia in male SNI rats by activating spinal SIRT1, which in turn enhances PGC-1α-mediated mitochondrial biogenesis and ATF5-induced UPR^{mt} (Fig. 15).

Existing studies have documented that CTRP3 participates in multiple biological processes, including inflammatory responses (30), glycolipid metabolism (29), oxidative stress regulation (26) and apoptotic pathways (46). For instance,

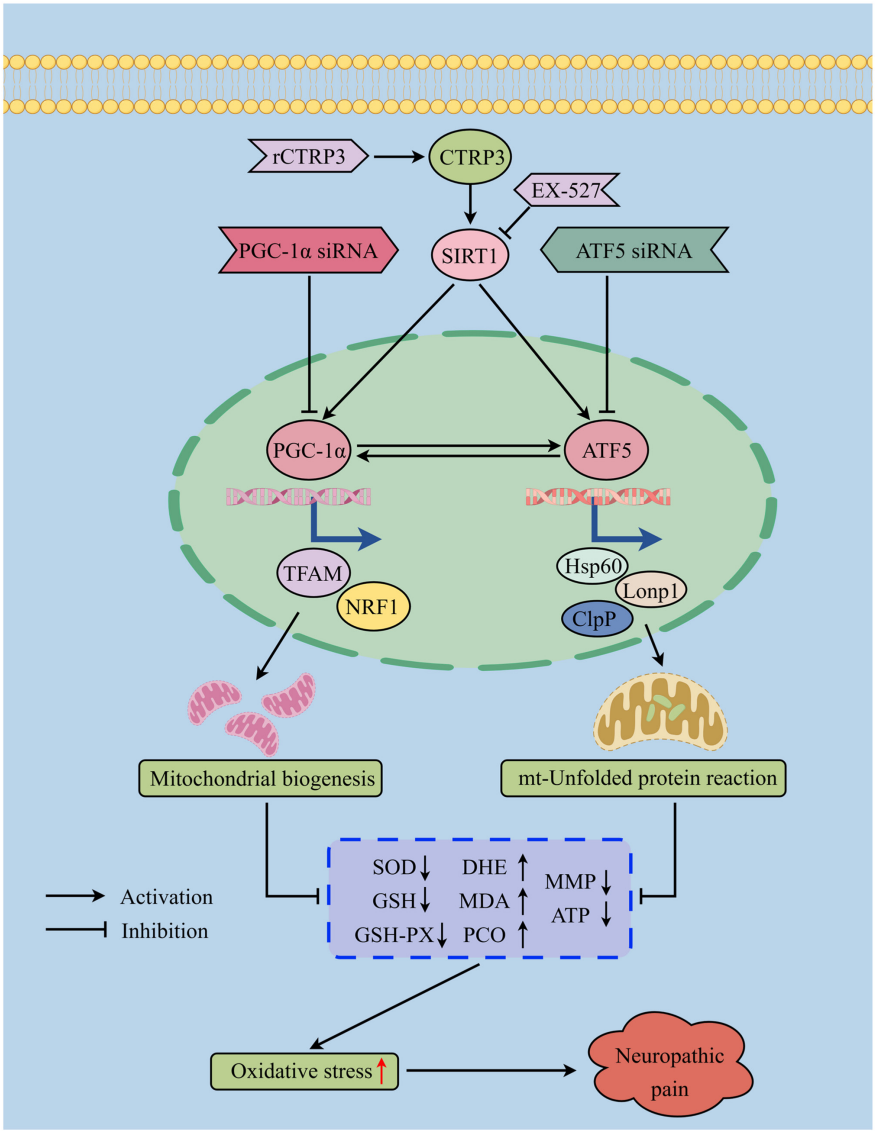

Figure 15. Schematic illustration of the role of CTRP3 in neuropathic pain. CTRP3 alleviates pain hypersensitivity and spinal oxidative stress in SNI rats by activating spinal SIRT1, thereby enhancing PGC-1α/ATF5-induced mitochondrial biogenesis and UPR^{mt}. CTRP3, complement C1q tumor necrosis factor-related protein 3; SNI, spared nerve injury; SIRT1, sirtuin 1; PGC-1α, peroxisome proliferator-activated receptor gamma coactivator 1-alpha; ATF5, activating transcription factor 5; UPR^{mt,} mitochondrial unfolded protein response; MDA, malondialdehyde; PCO, protein carbonyl; MMP, mitochondrial membrane potential; GSH, glutathione; GSH-PX, glutathione peroxidase; SOD, superoxide dismutase; DHE, dihydroethidium; ClpP, caseinolytic mitochondrial matrix peptidase proteolytic subunit; Hsp60, heat shock protein 60; LonP1, Lon protease 1; siRNA, small interfering RNA.

in inflammatory bowel disease, CTRP3 has been shown to reduce the phosphorylation of the NF-κB subunit p65 as well as the levels of proinflammatory cytokines such as tumor necrosis factor-α and interleukin-6, with this effect mediated through SIRT1 activation (30). In the field of cardiovascular research, CTRP3 exerts protective effects against apoptotic and oxidative stress-induced damage and alleviates myocardial ischemia/reperfusion injury via the LAMP1/JIP2/JNK signaling pathway (46). Additionally, CTRP3 can directly suppress inflammatory reactions in psoriatic keratinocytes by inhibiting the phosphorylation of signal transducer and activator of transcription 3 (STAT3) through LAMP1-dependent mechanisms (27). However, the specific role of CTRP3 in neuropathic pain remains incompletely understood. The present study found that SNI led to a significant downregulation of CTRP3 expression in spinal neurons. Although the precise mechanism by which peripheral nerve injury reduces spinal CTRP3 expression remains to be fully clarified, multiple transcriptional regulators may modulate CTRP3 expression under pathological conditions. Peripheral nerve injury triggers a cascade of pro-inflammatory, oxidative, ER stress, and hypoxic signals in the spinal cord, which may activate a series of negative transcriptional regulators (FOXO4 and KLF10) (47,48), and inhibitory microRNAs (miR-495-3p, miR-409-3p and miR-186-5p) (49-51) to reduce CTRP3 expression in the spinal cord. Furthermore, repeated intrathecal administration of rCTRP3 at doses of 30 and 90 μg significantly mitigated the reduction in PWT and attenuated the elevation in PWCD observed in male SNI rats. These results indicate that CTRP3 effectively alleviates mechanical allodynia and cold hyperalgesia in SNI-induced rats.

Mitochondrial biogenesis refers to the cellular process of generating new mitochondria to fulfill energy requirements and preserve organelle quality (6). This process is coordinated

by both nuclear and mitochondrial genes, with PGC-1α acting as a key transcriptional co-activator that upregulates NRF-1/2 and TFAM, thereby driving the expression of mtDNA and the assembly of respiratory chain complexes (7). Impaired mitochondrial biogenesis has been implicated in the pathogenesis of various diseases (9,15,36,52,53). For example, it has been reported that cardiomyocyte G protein-coupled receptor containing leucine-rich repeats 6 (LGR6) alleviates ferroptosis in diabetic cardiomyopathy by promoting mitochondrial biogenesis (52). Additionally, a study found that PGC-1α-mediated mitochondrial biogenesis enhances the recovery and survival of neuronal cells from degenerative damage (53). Our previous research also demonstrated that SNI-induced neuropathic pain suppresses mitochondrial biogenesis, while enhancing this process alleviates pain hypersensitivity (15,16,36). However, the specific mechanisms connecting mitochondrial biogenesis to neuropathic pain remain incompletely clarified. Another study indicated that CTRP3 mitigates neurological deficits in cerebral ischemic stroke by promoting PGC-1α-mediated mitochondrial biogenesis (32). Consistent with these findings, the present study revealed that PGC-1α siRNA blocked the rCTRP3-induced increase in PGC-1α expression in spinal dorsal horn neurons of SNI rats. WB analysis showed that PGC-1α siRNA abolished the rCTRP3-mediated upregulation of PGC-1α, NRF1 and TFAM in the spinal cord. Moreover, while rCTRP3 treatment reversed the reduction in mtDNA copy number in SNI rats, this effect was inhibited by PGC-1α siRNA. Furthermore, behavioral assessments demonstrated that rCTRP3 treatment ameliorated pain hypersensitivity in SNI rats, whereas co-administration of PGC-1α siRNA reversed this analgesic effect of rCTRP3. These results indicate that CTRP3 alleviates mechanical allodynia and cold hyperalgesia and promotes mitochondrial biogenesis in the spinal cord of SNI rats through PGC-1α activation.

Upon exposure to pathological stimuli, a hallmark of mitochondrial impairment is the perturbation of mitochondrial protein homeostasis, accompanied by the accumulation of unfolded or misfolded proteins within mitochondria. This accumulation not only elevates ROS levels but also triggers oxidative stress-induced injury, which in turn further compromises protein integrity and folding processes. Notably, activation of the UPR^{mt} acts as a protective mechanism for cell survival, facilitating proper protein folding or promoting the degradation of misfolded proteins. In mammalian cells, UPR^{mt} can be activated by multiple factors through diverse regulatory mechanisms, including via ATF5-a homolog of the ATFS-1 gene. ATF5 activation promotes the transcription of proteases (for example, ClpP and Lonp1) and heat shock proteins (for example, HSP60 and HSP10), which collectively aid in the correct folding or degradation of unfolded proteins, thereby restoring mitochondrial protein homeostasis. Impaired UPR^{mt} has been linked to the pathogenesis of various diseases. For example, a previous study demonstrated that enhancing UPR^{mt} with NR improved mitochondrial function, reduced chondrocyte death, and alleviated OA pain-effects that were markedly diminished in chondrocyte-specific Atf5 knockout mice (24). Additionally, ATF5-mediated UPR^{mt} has been shown to alleviate intervertebral disc degeneration by promoting mitophagy. However, strategies for safely and effectively regulating UPR^{mt} in pain hypersensitivity remain unclear, largely due to poorly understood underlying mechanisms. Another study indicated that CTRP3 mitigates mitochondrial dysfunction and oxidative stress injury in pathological cardiac hypertrophy by activating ATF5-induced UPR^{mt} (31). Consistent with this, the findings of the present study showed that ATF5 silencing via siRNA blocked the rCTRP3-induced upregulation of ATF5 in spinal dorsal horn neurons of SNI rats. Furthermore, RT-qPCR analysis revealed that ATF5 siRNA abolished the rCTRP3-mediated increases in spinal expression of proteases (ClpP and Lonp1) and heat shock proteins (Hsp60). Furthermore, the current data also demonstrated that rCTRP3 treatment dampened pain hypersensitivity in SNI rats, whereas co-administration of ATF5 siRNA reversed this analgesic effect. These data suggest that CTRP3 alleviates pain hypersensitivity and enhances UPR^{mt} in the spinal cord of SNI rats through ATF5 activation.

Next, the signaling pathways underlying CTRP3's analgesic effects and its regulatory role in mitochondrial function were investigated. SIRT1, a NAD^+-dependent protein deacetylase, has been widely studied in the field of neuropathic pain (54). It counteracts oxidative stress damage and mitochondrial dysfunction through multiple molecular or signaling pathways, while also exerting protective effects in neuropathic pain (55,56). Recent studies have shown that aberrant SIRT1 expression reduces PGC-1α-mediated mitochondrial biogenesis (34), and suppresses ATF5-induced UPR^{mt} (35). Furthermore, it has been reported that CTRP3 activates PGC-1α-induced mitochondrial biogenesis (32) and ATF5-mediated UPR^{mt} (31), thereby protecting mitochondria from proteotoxic damage and alleviating oxidative stress. A recent study demonstrated that CTRP3 mitigates mitochondrial dysfunction and enhances ATF5-induced UPR^{mt} in pathological cardiac hypertrophy by activating SIRT1 (31). Another study indicated that CTRP3 alleviated neurological deficits and promoted PGC-1α-mediated mitochondrial biogenesis in cerebral ischemic stroke by upregulating SIRT1 (32). Consistent with these findings, the present study showed that rCTRP3 treatment alleviated pain hypersensitivity in SNI rats, whereas co-administration of the SIRT1 antagonist EX-527 reversed this analgesic effect. IF staining revealed that EX-527 blocked the rCTRP3-induced upregulation of PGC-1α in spinal dorsal horn neurons of SNI rats. Moreover, while rCTRP3 treatment reversed the reduction in mtDNA copy number in SNI rats, this effect was abolished by EX-527. The present study also found that EX-527 inhibited the rCTRP3-induced increase in ATF5 expression in spinal dorsal horn neurons of SNI rats. Furthermore, RT-qPCR analysis demonstrated that EX-527 eliminated the rCTRP3-mediated upregulation of ClpP, Hsp60 and LonP1 in the spinal cord of rats with SNI. These results confirm that CTRP3 alleviates mechanical allodynia and cold hyperalgesia and promotes PGC-1α-mediated mitochondrial biogenesis and ATF5-induced UPR^{mt} in the spinal cord of SNI rats through SIRT1 activation.

Furthermore, previous studies have demonstrated that PGC-1α promotes ATF5-dependent UPR^{mt} (57), whereas ATF5 enhances the expression of PPARγ (58), a key positive transcriptional regulator of PGC-1α. In line with these observations, the present study revealed that PGC-1α silencing not only blocked rCTRP3-induced mitochondrial biogenesis but also significantly suppressed ATF5 and its downstream

UPR^{mt}-related markers. Similarly, ATF5 knockdown not only abolished rCTRP3-mediated UPR^{mt} activation but also significantly reduced PGC-1α and its downstream targets involved in mitochondrial biogenesis. Collectively, these findings confirm that PGC-1α and ATF5 mutually regulate each other downstream of SIRT1 during the analgesic action of CTRP3. This reciprocal interaction accounts for the similar reversal effects on neuropathic pain and oxidative stress observed following inhibition of SIRT1, PGC-1α, or ATF5. Our proposed signaling axis (CTRP3→SIRT1→PGC-1α/ATF5) is further supported, wherein PGC-1α and ATF5 function as interdependent downstream effectors rather than discrete parallel pathways.

Notably, it was previously reported by the authors that CTRP9 alleviates SNI-induced neuropathic pain in mice by modulating AdipoR1/AMPK/NF-κB signaling to suppress neuroinflammation and promote microglial M2 polarization (43). The present study extends these findings by demonstrating that CTRP3 exerts potent analgesic effects in rats via a distinct mechanism centered on SIRT1/PGC-1α/ATF5-mediated mitochondrial homeostasis, UPR^{mt} and oxidative stress inhibition. Several critical inter-species and molecular differences deserve emphasis. First, CTRP3 was downregulated in the spinal cord after SNI in rats, whereas CTRP9 was upregulated in mice, suggesting divergent expression patterns of CTRP family members in response to peripheral nerve injury across species. Second, the previous mouse study focused on microglial polarization and neuroinflammation, while the current rat study highlights mitochondrial dysfunction, mitochondrial biogenesis, UPR^{mt} and oxidative stress as core pathological events. Third, the downstream signaling differs substantially: CTRP9 acted through AdipoR1/AMPK/NF-κB in mice, whereas CTRP3 signals via SIRT1/PGC-1α/ATF5 in rats. These cross-species comparisons indicate that CTRP3 and CTRP9 function as complementary analgesic regulators with overlapping protective effects but distinct molecular cascades and expression patterns. Such species-specific regulatory features are critical for preclinical translation and suggest that CTRP3-targeted therapy may be more suitable for mitochondrial and oxidative stress-related pathological pain conditions in higher mammals.

Although the present study provides important insights into the role of CTRP3 in neuropathic pain, mitochondrial biogenesis and UPR^{mt}, several aspects warrant further exploration in future research. First, the study utilized rCTRP3, but its specificity and potential off-target effects in the context of neuropathic pain and mitochondrial function were not fully validated. Additional studies employing genetic knockdown or knockout approaches could help more definitively confirm the role of CTRP3. Second, the long-term effects of rCTRP3 treatment, including potential tolerance development or secondary changes over time, were not investigated. A longer follow-up period would provide a more comprehensive understanding of CTRP3's therapeutic potential. Additionally, only male rats were used in the present study, further studies are needed to explore potential sex differences in CTRP3 expression and function, as sex is a known modifier of neuropathic pain susceptibility and treatment response.

In summary, the present study demonstrates that CTRP3 mitigates pain hypersensitivity and spinal oxidative stress in male SNI rats by activating spinal SIRT1, thereby enhancing PGC-1α/ATF5-mediated mitochondrial biogenesis and UPR^{mt}. CTRP3 may thus represent a novel therapeutic target for the management of neuropathic pain.

Acknowledgements

The authors would like to thank the Laboratory Animal Center of Tongji Hospital, Tongji Medical College, Huazhong University of Science and Technology for their assistance in raising rats.

Funding

The present study was supported by the National Natural Science Foundation of China (grant nos. 82501492, 82471289 and 82271291).

Availability of data and materials

The data generated in the present study may be requested from the corresponding author.

Authors' contributions

TL designed the study. LZ provided experimental support. WM analyzed interpreted the data. TL and WM wrote the manuscript. TL and WM confirm the authenticity of all the raw data. All authors read and approved the final version of the manuscript.

Ethics approval and consent to participate

The present study was approved (approval no. TJH-202106615) by the Experimental Animal Care and Use Committee of Tongji Hospital, Tongji Medical College, Huazhong University of Science and Technology (Wuhan, China). All procedures were conducted in compliance with the Animal Research Reporting of in Vivo Experiments (ARRIVE) guidelines.

Patient consent for publication

Not applicable.

Competing interests

The authors declare that they have no competing interests.

References

1. Borbjerg MK, Wegeberg AM, Nikontovic A, Mørch CD, Arendt-Nielsen L, Ejskjaer N, Brock C, Vestergaard P and Røikjer J: Understanding the impact of diabetic peripheral neuropathy and neuropathic pain on quality of life and mental health in 6,960 people with diabetes. Diabetes Care 48: 588-595, 2025.
2. Soliman N, Moisset X, Ferraro MC, de Andrade DC, Baron R, Belton J, Bennett DLH, Calvo M, Dougherty P, Gilron I, *et al*: Pharmacotherapy and non-invasive neuromodulation for neuropathic pain: A systematic review and meta-analysis. Lancet Neurol 24: 413-428, 2025.
3. Su Y, Verkhratsky A and Yi C: Targeting connexins: Possible game changer in managing neuropathic pain? Trends Mol Med 30: 642-659, 2024.

4. Ward J, Grinstead A, Kemp A, Kersten P, Schmid AB and Ridehalgh C: A meta-analysis exploring the efficacy of neuropathic pain medication for low back pain or spine-related leg pain: Is efficacy dependent on the presence of neuropathic pain? Drugs 84: 1603-1636, 2024.
5. Malcangio M and Sideris-Lampretsas G: How microglia contribute to the induction and maintenance of neuropathic pain. Nat Rev Neurosci 26: 263-275, 2025.
6. Liu L, Li Y, Chen G and Chen Q: Crosstalk between mitochondrial biogenesis and mitophagy to maintain mitochondrial homeostasis. J Biomed Sci 30: 86, 2023.
7. Zhang L, Xin C, Wang S, Zhuo S, Zhu J, Li Z, Liu Y, Yang L and Chen Y: Lactate transported by MCT1 plays an active role in promoting mitochondrial biogenesis and enhancing TCA flux in skeletal muscle. Sci Adv 10: eadn4508, 2024.
8. Jamwal S, Blackburn JK and Elsworth JD: PPARγ/PGC1α signaling as a potential therapeutic target for mitochondrial biogenesis in neurodegenerative disorders. Pharmacol Ther 219: 107705, 2021.
9. Yang D, Sun Y, Wen P, Chen Y, Cao J, Sun X and Dong Y: Chronic stress-induced serotonin impairs intestinal epithelial cell mitochondrial biogenesis via the AMPK-PGC-1α axis. Int J Biol Sci 20: 4476-4495, 2024.
10. Dumesic PA, Wilensky SE, Bose S, Van Vranken JG, Gygi SP and Spiegelman BM: RBM43 controls PGC1α translation and a PGC1α-STING signaling axis. Cell Metab 37: 742-757.e8, 2025.
11. Lin H, Shao X, Gu H, Yu X, He L, Zhou J, Zhong Z, Guo S, Li D, Chen F, *et al*: Akkermansia muciniphila ameliorates doxorubicin-induced cardiotoxicity by regulating PPARα-dependent mitochondrial biogenesis. NPJ Biofilms Microbiomes 11: 86, 2025.
12. Lan X, Wang Q, Liu Y, You Q, Wei W, Zhu C, Hai D, Cai Z, Yu J, Zhang J and Liu N: Isoliquiritigenin alleviates cerebral ischemia-reperfusion injury by reducing oxidative stress and ameliorating mitochondrial dysfunction via activating the Nrf2 pathway. Redox Biol 77: 103406, 2024.
13. Wang W, Zhao F, Ma X, Perry G and Zhu X: Mitochondria dysfunction in the pathogenesis of Alzheimer's disease: Recent advances. Mol Neurodegener 15: 30, 2020.
14. Zheng Q, Liu H, Zhang H, Han Y, Yuan J, Wang T, Gao Y and Li Z: Ameliorating mitochondrial dysfunction of neurons by biomimetic targeting nanoparticles mediated mitochondrial biogenesis to boost the therapy of Parkinson's disease. Adv Sci (Weinh) 10: e2300758, 2023.
15. Zhang L, Tan X, Song F, Li D, Wu J, Gao S, Sun J, Liu D, Zhou Y and Mei W: Activation of G-protein-coupled receptor 39 reduces neuropathic pain in a rat model. Neural Regen Res 19: 687-696, 2024.
16. Zhang LQ, Zhou YQ, Li JY, Sun J, Zhang S, Wu JY, Gao SJ, Tian XB and Mei W: 5-HT_{1F} receptor agonist ameliorates mechanical allodynia in neuropathic pain via induction of mitochondrial biogenesis and suppression of neuroinflammation. Front Pharmacol 13: 834570, 2022.
17. Zhou Z, Fan Y, Zong R and Tan K: The mitochondrial unfolded protein response: A multitasking giant in the fight against human diseases. Ageing Res Rev 81: 101702, 2022.
18. Shpilka T and Haynes CM: The mitochondrial UPR: Mechanisms, physiological functions and implications in ageing. Nat Rev Mol Cell Biol 19: 109-120, 2018.
19. Sutandy FXR, Gößner I, Tascher G and Münch C: A cytosolic surveillance mechanism activates the mitochondrial UPR. Nature 618: 849-854, 2023.
20. Zu X, Chen S, Li Z, Hao L, Fu W, Zhang H, Yin Z, Wang Y and Wang J: SPI1 activates mitochondrial unfolded response signaling to inhibit chondrocyte senescence and relieves osteoarthritis. Bone Res 13: 47, 2025.
21. Xiong X, Hou J, Zheng Y, Jiang T, Zhao X, Cai J, Huang J, He H, Xu J, Qian S, *et al*: NAD^+-boosting agent nicotinamide mononucleotide potently improves mitochondria stress response in Alzheimer's disease via ATF4-dependent mitochondrial UPR. Cell Death Dis 15: 744, 2024.
22. An H, Zhou B, Hayakawa K, Durán Laforet V, Park JH, Nakamura Y, Mandeville ET, Liu N, Guo S, Yu Z, *et al*: ATF5-mediated mitochondrial unfolded protein response (UPR^{mt}) protects neurons against oxygen-glucose deprivation and cerebral ischemia. Stroke 55: 1904-1913, 2024.
23. Yang Y, Lu D, Wang M, Liu G, Feng Y, Ren Y, Sun X, Chen Z and Wang Z: Endoplasmic reticulum stress and the unfolded protein response: Emerging regulators in progression of traumatic brain injury. Cell Death Dis 15: 156, 2024.
24. Zhou Z, Lu J, Yang M, Cai J, Fu Q, Ma J and Zhu L: The mitochondrial unfolded protein response (UPR^{mt}) protects against osteoarthritis. Exp Mol Med 54: 1979-1990, 2022.
25. Xu WN, Zheng HL, Yang RZ, Sun YF, Peng BR, Liu C, Song J, Jiang SD and Zhu LX: The mitochondrial UPR induced by ATF5 attenuates intervertebral disc degeneration via cooperating with mitophagy. Cell Biol Toxicol 40: 16, 2024.
26. Wang Q, Piao J, Li Y, Tu H, Lv D, Hu L, Zhang R and Zhong Z: Bone marrow-mesenchymal stem cells alleviate microglial Pyroptosis after intracerebral hemorrhage in rat by secreting C1q/tumor necrosis factor-related protein 3. Exp Neurol 364: 114387, 2023.
27. Xue K, Shao S, Fang H, Ma L, Li C, Lu Z and Wang G: Adipocyte-derived CTRP3 exhibits anti-inflammatory effects via LAMP1-STAT3 axis in psoriasis. J Invest Dermatol 142: 1349-1359.e8, 2022.
28. Liu N, Gong Z, Li Y, Xu Y, Guo Y, Chen W, Sun X, Yin X and Liu W: CTRP3 inhibits myocardial fibrosis through the P2X7R-NLRP3 inflammasome pathway in SHR rats. J Hypertens 42: 315-328, 2024.
29. Yan Z, Cao X, Wang C, Liu S, Li Y, Lu G, Yan W, Guo R, Zhao D, Cao J and Xu Y: C1q/tumor necrosis factor-related protein-3 improves microvascular endothelial function in diabetes through the AMPK/eNOS/NO· signaling pathway. Biochem Pharmacol 195: 114745, 2022.
30. Yu H, Zhang Z, Li G, Feng Y, Xian L, Bakhsh F, Xu D, Xu C, Vong T, Wu B, *et al*: Adipokine C1q/tumor necrosis factor-related protein 3 (CTRP3) attenuates intestinal inflammation via sirtuin 1/NF-κB signaling. Cell Mol Gastroenterol Hepatol 15: 1000-1015, 2023.
31. Shi L, Tan Y, Zheng W, Cao G, Zhou H, Li P, Cui J, Song Y, Feng L, Li H, *et al*: CTRP3 alleviates mitochondrial dysfunction and oxidative stress injury in pathological cardiac hypertrophy by activating UPRmt via the SIRT1/ATF5 axis. Cell Death Discov 10: 53, 2024.
32. Gao J, Qian T and Wang W: CTRP3 activates the AMPK/SIRT1-PGC-1α pathway to protect mitochondrial biogenesis and functions in cerebral ischemic stroke. Neurochem Res 45: 3045-3058, 2020.
33. Luo Y, Ali T, Hu Y, Gong Q, Zheng C, Li L, Li S and Hao L: Erythropoietin (EPO) alleviates chronic stress-induced depression by modulating SIRT1-mediated mitochondrial function. J Neuroimmune Pharmacol 20: 73, 2025.
34. Liu Y, Yang H, Luo N, Fu Y, Qiu F, Pan Z, Li X, Jian W, Yang X, Xue Q, *et al*: An Fgr kinase inhibitor attenuates sepsis-associated encephalopathy by ameliorating mitochondrial dysfunction, oxidative stress, and neuroinflammation via the SIRT1/PGC-1α signaling pathway. J Transl Med 21: 486, 2023.
35. Li H, Chen D, Zhang X, Chen M, Zhi Y, Cui W, Li S, Xu F, Tan Y, Zhou H, *et al*: Screening of an FDA-approved compound library identifies apigenin for the treatment of myocardial injury. Int J Biol Sci 19: 5233-5244, 2023.
36. He Q, Zhou Y, Wu L, Huang L, Yuan Y, Flores JJ, Luo X, Tao Y, Chen X, Kanamaru H, *et al*: Inhibition of acid-sensing receptor GPR4 attenuates neuronal ferroptosis via RhoA/YAP signaling in a rat model of subarachnoid hemorrhage. Free Radic Biol Med 225: 333-345, 2024.
37. Xu Z, Xie W, Feng Y, Wang Y, Li X, Liu J, Xiong Y, He Y, Chen L, Liu G and Wu Q: Positive interaction between GPER and β-alanine in the dorsal root ganglion uncovers potential mechanisms: Mediating continuous neuronal sensitization and neuroinflammation responses in neuropathic pain. J Neuroinflammation 19: 164, 2022.
38. Zhang LQ, Gao SJ, Sun J, Li DY, Wu JY, Song FH, Liu DQ, Zhou YQ and Mei W: DKK3 ameliorates neuropathic pain via inhibiting ASK-1/JNK/p-38-mediated microglia polarization and neuroinflammation. J Neuroinflammation 19: 129, 2022.
39. Zhao Y, Zhang Y, Lei T, Zhang S, Nan K, Zhang X and Fan LH: ZEB1 maintains mitochondrial fission and macrophage efferocytosis by restraining MFN2, thereby limiting inflammation and improving tendon-bone healing. Int J Mol Med 57: 134, 2026.
40. Li L, Bai L, Yang K, Zhang J, Gao Y, Jiang M, Yang Y, Zhang X, Wang L, Wang X, *et al*: KDM6B epigenetically regulated-interleukin-6 expression in the dorsal root ganglia and spinal dorsal horn contributes to the development and maintenance of neuropathic pain following peripheral nerve injury in male rats. Brain Behav Immun 98: 265-282, 2021.
41. Fan CY, McAllister BB, Stokes-Heck S, Harding EK, Pereira de Vasconcelos A, Mah LK, Lima LV, van den Hoogen NJ, Rosen SF, Ham B, *et al*: Divergent sex-specific pannexin-1 mechanisms in microglia and T cells underlie neuropathic pain. Neuron 113: 896-911.e9, 2025.

42. Zhang L, Dai X, Li D, Wu J, Gao S, Song F, Liu L, Zhou Y, Liu D and Mei W: MFG-E8 ameliorates nerve injury-induced neuropathic pain by regulating microglial polarization and neuroinflammation via integrin β3/SOCS3/STAT3 pathway in mice. J Neuroimmune Pharmacol 19: 49, 2024.
43. Liu T, Zhang L and Mei W: CTRP9 attenuates peripheral nerve injury-induced mechanical allodynia and thermal hyperalgesia through regulating spinal microglial polarization and neuroinflammation mediated by AdipoR1 in male mice. Cell Biol Toxicol 40: 91, 2024.
44. Yingze Y, Zhihong J, Tong J, Yina L, Zhi Z, Xu Z, Xiaoxing X and Lijuan G: NOX2-mediated reactive oxygen species are double-edged swords in focal cerebral ischemia in mice. J Neuroinflammation 19: 184, 2022.
45. Zhang H, Zhang N, Yang X, Zhang J, Ge X, Wang L, Wang S and Wen Y: DL-3-n-butylphthalide protects mitochondria against ischemia/hypoxia damage via suppressing GCN5L1-mediated Drp1 acetylation in neurons and mouse brains. CNS Neurosci Ther 31: e70682, 2025.
46. Song Y, Zhang Y, Wan Z, Pan J, Gao F, Li F, Zhou J and Chen J: CTRP3 alleviates myocardial ischemia/reperfusion injury in mice through activating LAMP1/JIP2/JNK pathway. Int Immunopharmacol 107: 108681, 2022.
47. Zeng X, Peng Y, Wang Y and Kang K: C1q/tumor necrosis factor-related protein-3 (CTRP3) activated by forkhead box O4 (FOXO4) down-regulation protects retinal pericytes against high glucose-induced oxidative damage through nuclear factor erythroid 2-related factor 2 (Nrf2)/Nuclear factor-kappaB (NF-κB) signaling. Bioengineered 13: 6080-6091, 2022.
48. Zeng Y, Xu Y, Pan Y and Guo H: KLF10 knockdown negatively regulates CTRP3 to improve OGD/R-induced brain microvascular endothelial cell injury and barrier dysfunction through Nrf2/HO-1 signaling pathway. Tissue Cell 82: 102106, 2023.
49. Chen Y, Liu W, Chen M, Sun Q, Chen H and Li Y: Up-regulating lncRNA OIP5-AS1 protects neuron injury against cerebral hypoxia-ischemia induced inflammation and oxidative stress in microglia/macrophage through activating CTRP3 via sponging miR-186-5p. Int Immunopharmacol 92: 107339, 2021.
50. Wu T, Tang C, Fan J and Tao J: Administration of rTMS alleviates stroke-induced cognitive deficits by modulating miR-409-3p/CTRP3/AMPK/Sirt1 axis. J Mol Neurosci 72: 507-515, 2022.
51. Zhao G, Zhang L, Qian D, Sun Y and Liu W: miR-495-3p inhibits the cell proliferation, invasion and migration of osteosarcoma by targeting C1q/TNF-related protein 3. Onco Targets Ther 12: 6133-6143, 2019.
52. Zhao M, Shen Z, Zheng Z, Xu Y, Zhang J, Liu J, Peng S, Wan J, Qin JJ and Wang M: Cardiomyocyte LGR6 alleviates ferroptosis in diabetic cardiomyopathy via regulating mitochondrial biogenesis. Metabolism 159: 155979, 2024.
53. You W, Knoops K, Berendschot TTJM, Benedikter BJ, Webers CAB, Reutelingsperger CPM and Gorgels TGMF: PGC-1a mediated mitochondrial biogenesis promotes recovery and survival of neuronal cells from cellular degeneration. Cell Death Discov 10: 180, 2024.
54. Song FH, Liu DQ, Zhou YQ and Mei W: SIRT1: A promising therapeutic target for chronic pain. CNS Neurosci Ther 28: 818-828, 2022.
55. Xu JW, Xu X, Ling Y, Wang YC, Huang YJ, Yang JZ, Wang JY and Shen X: Vincamine as an agonist of G-protein-coupled receptor 40 effectively ameliorates diabetic peripheral neuropathy in mice. Acta Pharmacol Sin 44: 2388-2403, 2023.
56. Pal A, Sharan L, Das A, Paul S, Babu SS, Das S, Banerjee S and Kumar A: Vitexin mitigates AIM2 inflammasome-mediated mitochondrial dysfunction and neuroinflammation in chronic constriction injury induced neuropathy model. Int Immunopharmacol 158: 114877, 2025.
57. Zhang B, Tan Y, Zhang Z, Feng P, Ding W, Wang Q, Liang H, Duan W, Wang X, Yu S, *et al*: Novel PGC-1α/ATF5 axis partly activates UPR^{mt} and mediates cardioprotective role of tetrahydrocurcumin in pathological cardiac hypertrophy. Oxid Med Cell Longev 2020: 9187065, 2020.
58. Zhao Y, Zhang YD, Zhang YY, Qian SW, Zhang ZC, Li SF, Guo L, Liu Y, Wen B, Lei QY, *et al*: p300-dependent acetylation of activating transcription factor 5 enhances C/EBPβ transactivation of C/EBPα during 3T3-L1 differentiation. Mol Cell Biol 34: 315-324, 2014.